Advanced Branching Control and Characterization of Inorganic Semiconducting Nanocrystals

By

Steven Michael Hughes

B.A. (Connecticut College) 2002

A dissertation submitted in partial satisfaction of the requirements for the degree of

Doctor of Philosophy

in

Chemistry

in the

Graduate Division

of the

University of California, Berkeley

Committee in charge:

Professor A. Paul Alivisatos, Chair

Professor Gabor A. Somorjai

Professor Ronald Gronsky

Fall 2007

Advanced Branching Control and Characterization of

Inorganic Semiconducting Nanocrystals

Steven Michael Hughes

Abstract

Advanced Branching Control and Characterization of

Inorganic Semiconducting Nanocrystals

by

Steven Michael Hughes

Doctor of Philosophy in Chemistry

University of California, Berkeley

Professor A. Paul Alivisatos, Chair

The ability to finely tune the size and shape of inorganic semiconducting nanocrystals is an area of great interest[1-5], as the more control one has, the more applications will be possible for their use. The first two basic shapes developed in nanocrystals were the sphere[6-8] and the anisotropic nanorod[1, 9]. The II-VI materials being used such as Cadmium Selenide (CdSe) and Cadmium Telluride (CdTe), exhibit polytypism, which allows them to form in either the hexagonally packed wurtzite or cubically packed zinc blende crystalline phase[10, 11]. The nanorods are wurtzite with the length of the rod growing along the c-axis[1]. As this grows, stacking faults may form, which are layers of zinc blende in the otherwise wurtzite crystal. Using this polytypism, though, the first generation of branched crystals were developed in the form of the CdTe tetrapod[12]. This is a nanocrystal that nucleates in the zincblend form, creating a tetrahedral core, on which four wurtzite arms are grown. This structure opened up the possibility of even more complex shapes and applications. This dissertation investigates

the advancement of branching control and further understanding the materials' polytypism in the form of the stacking faults in nanorods.

Understanding the nature of the polytypism in these materials is paramount to controlling their branching. Thus the first step is understanding the formation of stacking faults, which are the most common appearance of polytypism in these materials. By performing a thorough statistically analysis of the growth of stacking faults in these rods, a better understanding is obtained on how and where the faults form, and how best to encourage branching. With this knowledge, more complex structures begin to make more sense, such as heterostructures. The semiconductor heterstructures developed here incorporate multiple materials into a single nanocrystal. Additionally, they can incorporate a second generation of branching as well to form even more complex structures. One example of such a structure is a CdSe tetrapod with branching CdTe at the end of each original rod, resulting in a nanocrystal with a total of 12 arms. In addition to this method, oriented attachment is also investigated here as a viable means of branching. Using this technique, gold is used as an intermediate method of attachment for two CdSe rods. Once the gold joint is ultimately removed a new piece of CdSe is grown between the two original rods, and its crystalline phase appears to be dictated by the angle and orientation of the joining rods. Through these methods of crystalline growth and characterization new progress is made toward the ultimate goal of complete structural control over materials such as these II-VI semiconductor nanocrystals.

Acknowledgements

No work such as this can be done alone, and as such there are many people who deserve thanks for both getting me to this point and keeping me going. I'd like to begin by thanking my wife, Amy, and my parents for having helped encourage me along the way and to make sure I never gave up.

At work and at play, my coworkers and friends have been a huge help and have always been there to remind me that experiments don't always go the way they're supposed to; that's just science for you. I'd especially like to acknowledge Alex Mastroianni and Josh Wittenberg, my classmates in the Alivisatos Group. It's been a long run, but you guys have really helped make it fun.

Last but not least, I'd like to thank my Advisor, Paul Alivisatos. You were willing to take me into your group, give me a TEM, and let me run with my ideas. Without your trust and vision, none of this could have been.

Thank you.

Dedication

I would like to dedicate this work to my father, who instilled in me a love of science, and to my grandfather who showed me that learning never ends.

Table of Contents

Chapter 1. Introduction 1

1.1. Looking Towards the Future 1

1.2. Methodologies 2

1.3. Nanoscale Properties 3

1.4. Shape and Size Control as a Means for Greater Integration 4

1.5. Dissertation's Outline 5

Chapter 2. Experimental Methods 7

2.1. Synthetic Methods 7

2.1.1. Introduction to Shape Control 7

2.1.2. Rod Synthesis 11

2.1.3. Rod Variations 11

2.1.4. Basic Heterostructure Synthesis 15

2.1.5. Cleaning 15

2.1.6. Gold Tipping CdSe Nanorods 15

2.2. Methods of Characterization 18

2.2.1. Transmission Electron Microscopy 18

Introduction 18

Instrument and preparation 21

2.2.2. X-ray Electron Dispersive Spectroscopy 21

2.2.3. Optical Characterization 22

Chapter 3. Polytypism and Stacking Fault Formation 24

3.1. Introduction 24
3.2. Experimental Methods 25
3.3. Varying Rod Length 28
3.3.1. Experiment and Results 28
3.3.2. Discussion 30
3.4. Stacking Fault Growth Evolution 31
3.4.1. Experiment and results 31
3.4.2. Discussion 33
3.5. Generality 35
3.5.1. Experiment and Results 35
3.5.2. Discussion 35
3.6. Conclusions 36
Chapter 4. Heterostructures 37
4.1. Introduction 37
4.2. Heterostructure Background 38
4.3. Synthetic Methods 42
4.4. Characterization 45
4.4.1. EDS 45
4.4.2. TEM statistics 49
4.4.3. Optical 49
4.4.4. HRTEM 52
4.4.5. Branched Rod Growth Directions 54
4.4.6. Theoretical Models 56

4.5. Conclusion 60

Chapter 5. Oriented Attachment 62

5.1. Introduction 62

5.2. Synthetic Methods 62

5.3. Attachment Characterization 66

5.3.1. Presence of Gold 66

5.3.2. Orientation of Gold Tipping 66

5.3.3. Attachment Directionality 69

5.3.4. Distribution of Angles Before and After Attachment 71

5.3.5. Possible Heterostructure Formation 73

5.4. Conclusion 75

Chapter 6. Concluding Remarks 76

References 79

Chapter 1. Introduction

1.1. Looking Towards the Future

The world we live in increasingly craves the latest technology in every aspect of our life: all work and presentations are done on desktop or laptop computers; communication is done via emails and cell phones; and for leisure, music players that contain thousands of songs are indispensable. It does not stop at computing though. A pair of slacks advertises its use of nanotechnology to prevent stains, while sunscreen uses nanoparticles to absorb a range of ultraviolet light and protect your skin. All of these share one thing in common; they are pushing current technology to be smaller and smaller. For manufacturers, the goal is to make it so the user doesn't need to how something works, only that it does. With the advent of nanotechnology, scientists and engineers are working with materials far smaller than the eye can see, so many users may never know how their cell phones or stain resistant pants work unless they bother to ask.

The materials that will be studied in the following pages are types of II-VI inorganic semiconducting nanocrystals[13, 14]. In the semiconductor industry, smaller is better for multiple reasons. As we miniaturize our materials, more circuitry can be crammed onto a smaller area, power consumption is decreased and computing ability is increased[15]. And at this time nanocrystals are about as small as semiconductors come, generally ranging in size from 3 to 100 nm in any given dimension. The greatest challenge of course, is control. How does one make, process, and characterize materials

that are only hundreds of atoms large? Current methods are being pushed to their limits and newer ones are needed to pick up where the previous generation leaves off.

1.2. Methodologies

The two basic approaches to any material's development in general are the top down and bottom up methods. These refer to the direction in which the form of the final material is made. In the top down approach, material is removed from a larger sample until the final shape and size desired are obtained. One example of this method is electron beam lithography[15, 16]. In e-beam lithography a pattern is created using an electron beam on a sensitive surface. The material that has been exposed is now chemically different from the unexposed regions, and each section can subsequently be processed and removed differently. This leaves only the desired material on the final surface. This widely used technique is used to create circuit patterns on silicon wafers.

The bottom up approach meanwhile starts with atomic or molecular precursors and grows the desired material directly. An example of this method would be colloidal syntheses such as the ones used in this research[2, 17, 18]. There are many variations of colloidal syntheses, some in aqueous solutions others in organic solvents[19]. In all of these syntheses however, the basic principle is the same; crystals are nucleated in a solution of precursor monomers and grown to the desired extent. The shape and size of the crystals are often determined by either growth in micelles[19-21] or the presence of surfactants that selectively bind crystalline facets[1, 22]. The growth can be easily tuned by temperature, concentration, and reaction mixture. In addition to being highly tunable, these syntheses also have the advantage of being more easily scaled up and solution processable[17].

1.3. Nanoscale Properties

One of the most interesting effects of making new materials on the order of nanometers is that the properties of the materials begin to change. Physically, the materials are now made up of only hundreds of atoms, the result is that the surface and edge atoms now make up a far greater fraction of the total atoms in the particle. Because the surface atoms have dangling bonds that are less well passivated than an inner atom that is fully coordinated, these atoms have a higher energy and will more readily react to external perturbations, whether mechanical[23] or chemical[24, 25]. Because of this, the entire particle will behave differently than the bulk material[25]. For instance the melting point of the materials drop[14] and chemical reactivity increases. Electronically, the size of the materials are now down to the size where they may actually be smaller than the bohr radius of their electron, thereby confining the exciton[14, 26]. For a nanocrystal, this quantum confinement can be described by the particle in a box equations. The smallest dimension of the nanocrystal defines the size of the box, so when the size of the crystal is decreased the box is shrunk and the confinement of the exciton increases. This results in the increased separation of the energy levels in the nanocrystal[19]. While at first this may seem like an undesirable effect, and to some it may be, the ability to tune the semiconductor's bandgap by this method can lead to all new uses and fields of study for this class of material. For instance, in the classic example of cadmium selenide (CdSe) nanodot emission, the semiconductor can be tuned to emit anywhere from blue to red light, simple by changing the size of the crystals[27].

1.4. Shape and Size Control as a Means for Greater Integration

The ability to finely tune the size and shape of inorganic semiconducting nanocrystals is an area of great interest, as the more control one has, the more applications will be possible for their use. The need for size control is clear from the previous example. If one wishes to tune the bandgap of a material carefully at this size, very fine control is needed. The need for shape control is immediately apparent when one considers the logistics of integrating these materials into other systems for real applications[28]. The first two basic shapes developed in nanocrystals were the sphere and the anisotropic nanorod. The spherical nanodot was difficult for circuit integration, but is still a very relevant shape for certain biological uses[29]. The rod, however, was a big advancement for these materials, and has indeed led to better integration methods[30]. However, the rod was limited to essentially having only two leads that could be used, the two ends of the rod. The need to make more complex branched structures was readily apparent.

The II-VI materials being used such as Cadmium Selenide (CdSe) and Cadmium Telluride (CdTe), exhibit polytypism, which allows them to form in either the hexagonally packed wurtzite or cubically packed zinc blende crystalline phase[10]. The nanorods are wurtzite with the length of the rod growing along the c-axis. As this grows, stacking faults may form, which are layers of zinc blende in the otherwise wurtzite crystal. Using this polytypism, though, the first generation of branched crystals were developed in the form of the CdTe tetrapod[12]. This is a nanocrystal that nucleates in the zincblend form, creating a tetrahedral core, on which four wurtzite arms are grown. Now

there were all new possibilities opening up for these nanocrystals[31]. Yet, the one thing the tetrapods truly demonstrated was the desire for even more complex structures.

1.5. Dissertation's Outline

The characterization of nanomaterial's physical[14], electronic[31], magnetic[32], and optical[33] properties has been a vast area of research for the last couple decades and shows no sign of ending any time soon. This dissertation will cover my research on the characterization of stacking fault formation in nanorods, along with the developement of new techniques for the formation and characterization of advanced branched semiconductor nanocrystals. The two principle materials that will be used throughout this dissertation are cadmium selenide (CdSe) and cadmium telluride (CdTe), and to a lesser extent cadmium sulfide (CdS). Chapter 2 will outline the experimental methods used to grow and characterize these materials. The basic synthetic techniques used throughout all the experiments will be presented here, along with the commonly used methods to tune the growth of the crystals for such attributes as increased branching or increased thickness. General background on the primary instruments used during these experiments will also be presented in this chapter. Chapter 3 is on the analysis of the stacking faults in nanorods. These stacking faults arise due to the polytypism of the materials. By a careful observation and analysis of stacking faults in these materials much can be gleamed about their growth behavior. In Chapter 4, the formation of linear and branched heterostructures by the addition of a second material during growth will be explored. During this growth, branched structures may form in part due to the polytypism of the materials, and the ease with which they form either crystalline phase.

These materials are especially interesting because of their charge separation abitlity. This chapter is largely reproduced with permission from the journal and all authors from the previously published journal article: Milliron, D.J.; Hughes, S.M.; Cui, Y.; Manna, L.; Li, J.B.; Wang, L.W.; Alivisatos, A.P. "Colloidal nanocrystal heterostructures with linear and branched topology" *Nature* **2004**, 430, 190-195. Chapter 5 will discuss an alternative method for branching via oriented attachment. This technique offers both advantages and disadvantages to the former branching method, and both will be outlined here. Finally, in Chapter 6, the advances in the field from this research will be summarized, concluding what has been found during this research and how it may be advanced in the future.

Chapter 2. Experimental Methods

2.1. Synthetic Methods

2.1.1. Introduction to Shape Control

The shape control of nanomaterials has long been an area of intense investigation[1, 3, 12]. The ability to alter the shape of the materials can lead to an increasing number of applications[29, 34, 35]. Originally, these materials were grown in the most basic shape, a sphere, and it was only by accident, as so many discoveries are made, that the anisotropic nanorod was developed. As is true with many chemicals, there are often impurities, in this case there were phosphonic acids in the technical grade tri(n-octyl)phosphine oxide (TOPO) that was being used as the organic solvent for the spherical nanocrystals. The introduction of these phosphonic acids led to the anisotropic growth of nanorods[1]. In a rod growth, these phosphonic acids selectively bind to the side facets of the nanorod, leading to increased growth along the c-axis of the rod, as shown in Figure 1. The (001) and (00-1) faces, however, are not chemically equivalent. If we assume that both faces are not passivated and capped with cadmium, then the (001) face will have a single dangling bond exposed, while the (00-1) face will have three dangling bonds. It is because of this anisotropy that the (001) face is considered slow growing, and the (00-1) face, much more difficult to passivate with three times as many dangling bonds, is taken to be the fast growing face.

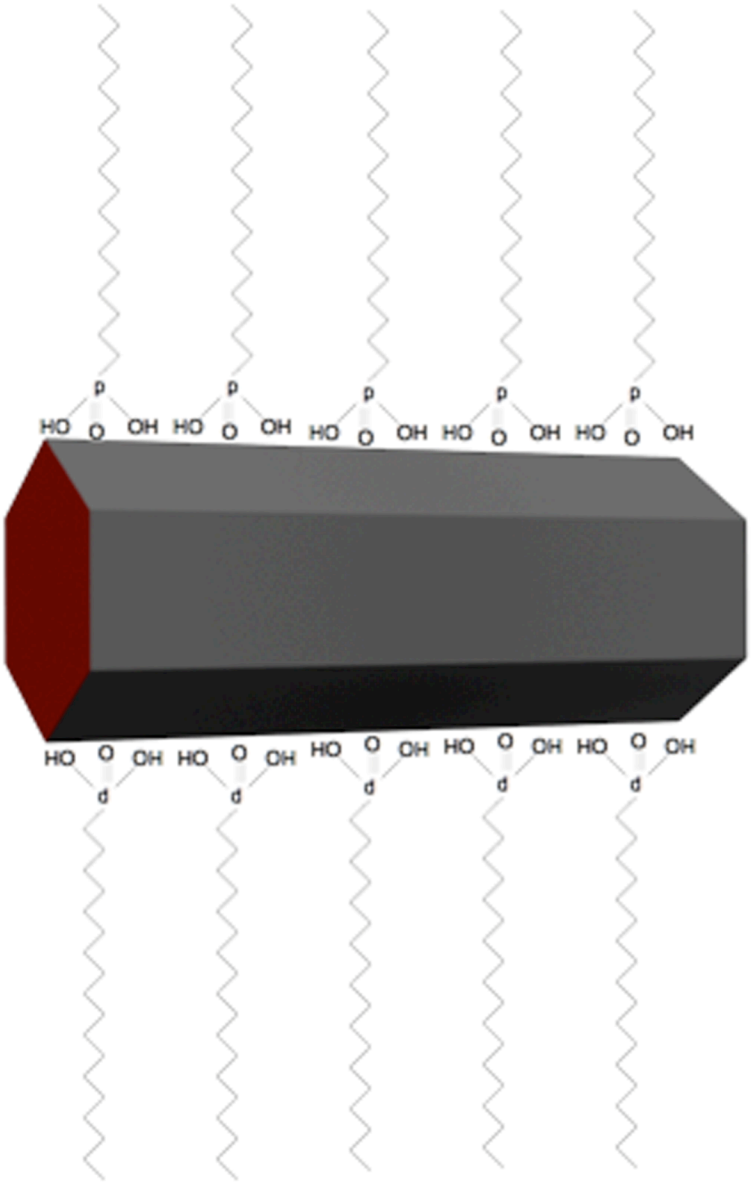

Figure 1. A model of a CdSe nanorod. The side facets of the nanorod are passivated with Octadecylphosphonic Acid (ODPA), which leads to the preferential growth of the +/-(001) faces at the ends of the rod, colored red here.

Shortly after the development of the nanorod it was found that by encouraging nucleation in the zinc blende phase a new shape of crystal could be formed, namely the tetrapod[12]. In this crystal, the core of the structure is a tetrahedral piece of zinc blende with four equivalent (111) faces. These (111) faces are packed similarly and are chemically equivalent to the +/-(001) faces in the wurtzite structure, with alternating layers of cadmium and the anion being used such tellurium. Because of this, once the core reaches a certain size, it becomes more energetically favorable for wurtzite arms to grow off of the four zinc blende faces, since the wurtzite structure is better passivated by present ligands. This basic branching structure is shown in Figure 2.

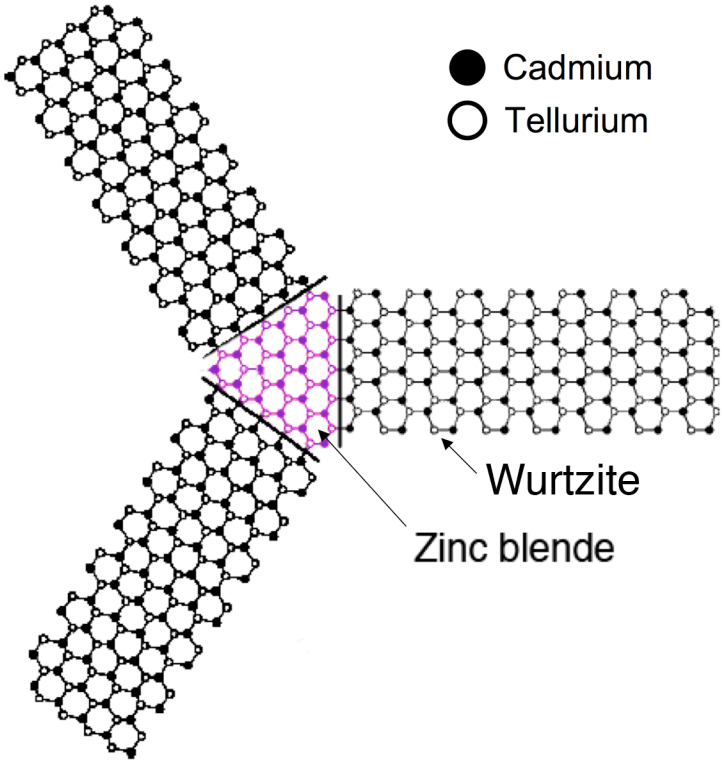

Figure 2. At tetrapod consisting of four wurtzite arms grown off of a zinc blende core with four equivalent (111) faces. The fourth arm is not shown as it would be growing perpindicular to the plane of the image.

2.1.2. Rod Synthesis

Rods were grown by making small variations to a standard recipe. The rods were grown in a 50 mL three neck round bottom flask attached to a schlenk line by a short condenser. In one of the two remaining necks a thermocouple adapter was used so not to contaminate the reaction mixture, and a rubber septa was placed in the final neck for injections. The reaction was heated with a heating mantle attached to a controller, Figure 3. A reactant mixture of 200 mg CdO, 2.98 g tri(n-octyl)phosphine oxide (TOPO), 0.94 g Octadecylphosphonic Acid (ODPA), and 0.05 g Hexylphosphonic Acid (HPA) were heated to 120 ^{o}C under vacuum to degas after melting. An overall ratio of two phosphonic acid molecules per cadmium atom was found to be ideal. The temperature was increased slowly to 300 ^{o}C to decompose the CdO. The now clear solution was lowered after 10 min to 120 ^{o}C for a second degassing of 1 – 2 hrs. The mixture was heated to its reaction temperature, between 260 – 320 ^{o}C, and the anion precursor, a Se – tri(n-octyl)phosphine complex, was injected. The growth was allowed to continue for 5 minutes before the heating mantel was removed.

2.1.3. Rod Variations

Growing a batch of nanocrystals can at times feel like more of an art than a science. It takes only a small perturbation in the synthesis to change the results. Figure 4 showcases two rod syntheses that resulted in very different rods despite similar growth conditions. The primary factors to watch in a synthesis are the concentrations of

reactants, temperature, and surfactant chain length. Concentration is the most difficult factor to predict the results with. If the concentration of reactants is increased one of two things may occur. If the concentration of reactants is increased to add material to the synthesis and the nucleation event does not change, then the crystals should increase in size. However, if the concentration is too high, there may be an increase in nucleation. In this case, because there are more nucleation events, the amount of material per crystal will be less, and the final nanocrystals will be smaller than before.

The results of the second factor, temperature, are easier to predict. During nucleation, a higher temperature will result in greater nucleation and smaller crystals. Additionally, during growth, higher temperatures lead to less branching. As a standard, 300 ^{o}C is a good temperature for larger rods with little branching. For increased branching, 260 ^{o}C will give larger and highly faulted rods.

Finally, the chain length of the surfactants play a very large role in rod shape and size. As has been noted before, using only a loosely binding surfactant such as TOPO will lead to spherical particles. The addition of stronger binding surfactants such as long chain phosphonic acids results in the growth of nanorods. For a nanorod with a diameter of 8 nm is desired, then a surfactant such as ODPA is used with a chain length of 18 carbons. For narrower rods, the addition of small amounts of short chain phosphonic acids greatly helps. Adding as little as 5% Hexylphosphonic Acid (HPA) of the total phosphonic acids in the solution, will result in thinner and longer rods. However if the concentration of short chain surfactants is too high there will be an increase in uncontrolled branching and more stacking faults in the rods. The addition of shorter chains will also benefit the growth of tetrapods if that is the desired product.

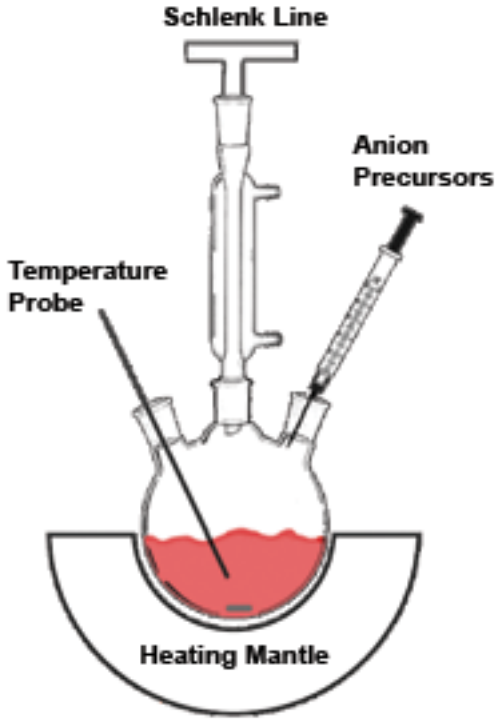

Figure 3. The standard synthesis setup consists of a three-neck flask and condenser hooked up to a schlenk line for air free syntheses. The reaction mixture is heated with a heating mantle, while the temperature is monitored using a thermocouple temperature probe. To begin the crystal growth an anion precursor solution is rapidly injected by syringe.

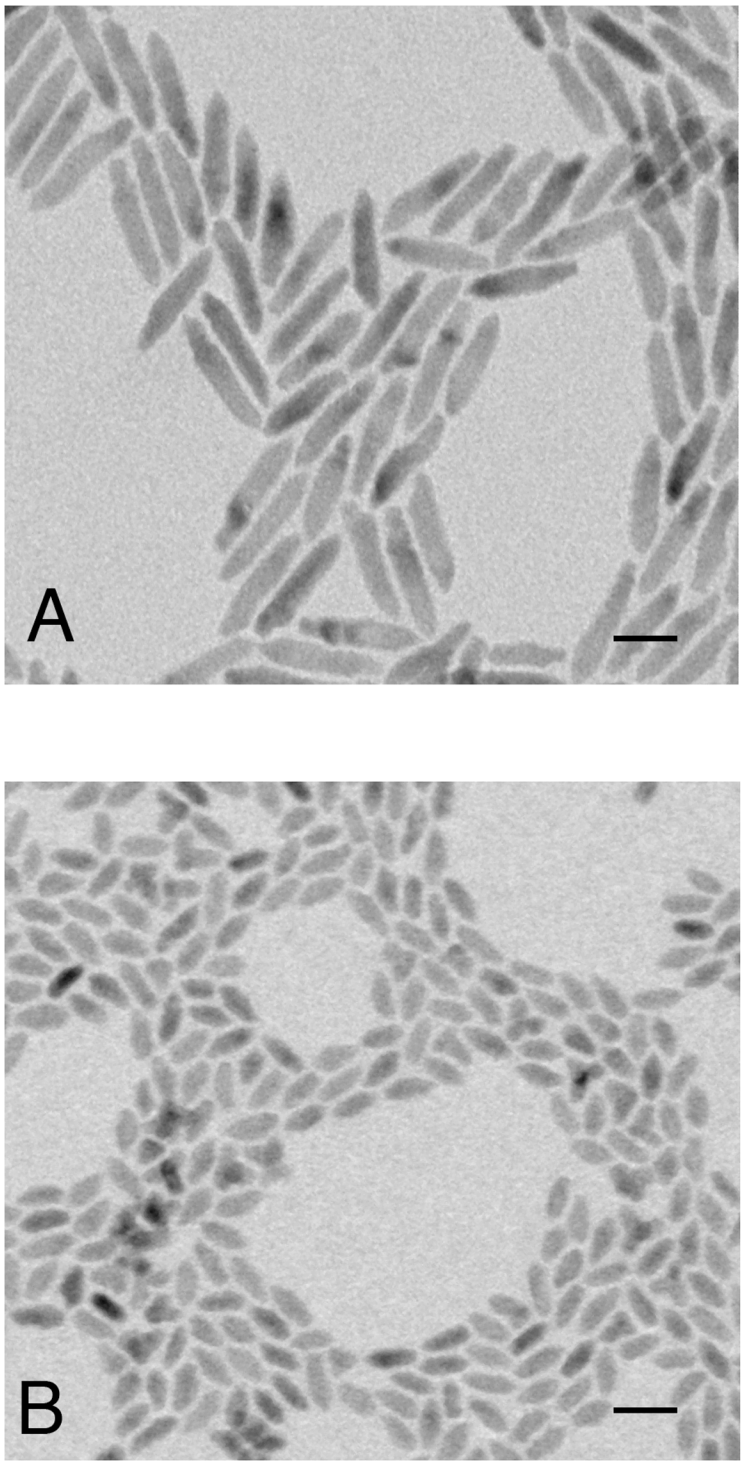

Figure 4. Transmission electron micrographs of two batches of rods grown under similar conditions. The scale bar in each is 20 nm.

2.1.4. Basic Heterostructure Synthesis

In a typical preparation for CdSe/CdTe branched rod heterostroctures, 104 mg of CdO was dissolved in 0.81 g of octadecylphosphonic acid (PolyCarbon Industries) and 3.19 g of tri(n-octyl)phosphine oxide at 300ºC under air–free conditions. At 280ºC, 15.8 mg of selenium dissolved in 320 mg of tri(n-octyl)phosphine (TOP) were injected and the CdSe nanorods grew for four minutes. Then, at 290ºC, 34 mg of tellurium dissolved in 306 mg of TOP were injected and CdTe branches grew for six minutes before the heat was removed to stop the reaction.

2.1.5. Cleaning

Once the reaction mixtures have cooled to room temperature the crystal growth has ended, and the final product must be isolated from the remaining unreacted starting materials. To do this the crystals were selectively precipitated and centrifuged out. Methanol or isopropanol was added until the colloidal solution became cloudy due to precipitation. At this point the solution was centrifuged for approximately 5 minutes at 3000 rpm. The unwanted solution was decanted off, and the crystals were resuspended in toluene or chloroform. This procedure was repeated three times for any given batch of nanorods.

2.1.6. Gold Tipping CdSe Nanorods

For growing gold tips on CdSe nanorods, a single batch of rods, approximately 75 mg, is diluted in 12 g of Toluene and stirred at room temperature. To this, 4 mL of a

solution containing 12 mg $AuCl_3$, 45 mg Hexyldecylamine (HDA), and 25 mg Didodecyldimethyl-ammonium bromide (DDAB) in 5 g Toluene is slowly added dropwise at a rate of 0.2 mL/min. After the addition is complete the solution is cleaned as normal to remove any unreacted reagents. This procedure results in rods with 2-5 nm gold tips on each end. To obtain rods with only a single tip, a similar procedure may be followed, adding only 2 mL of the reaction mixture at 0.02 mL/min. Figure 5 is a micrograph of typical results for a standard gold tipping procedure.

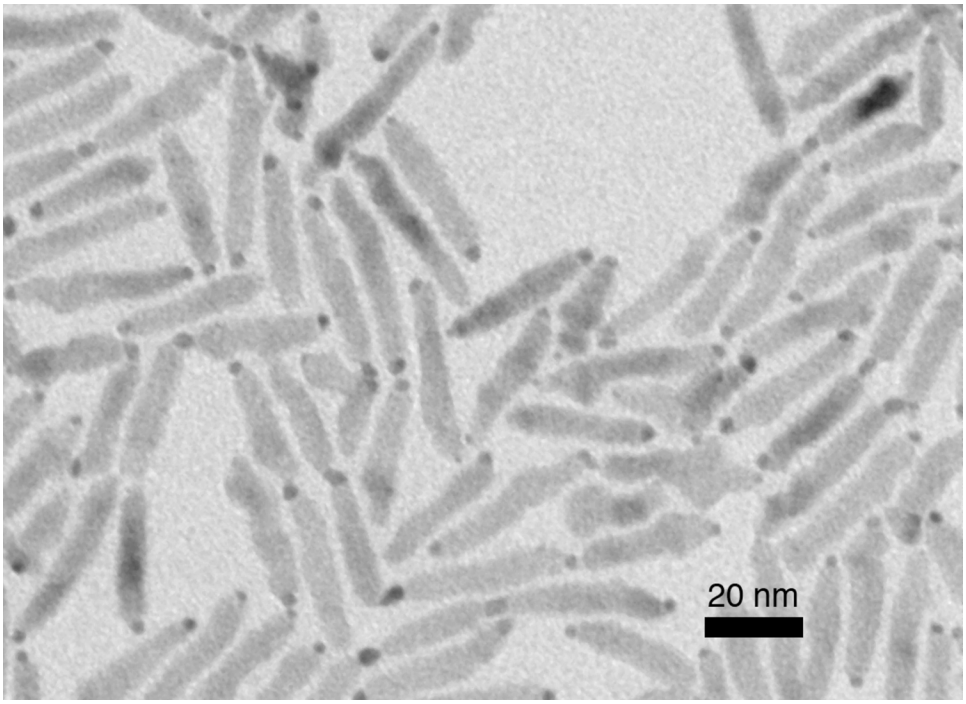

Figure 5. A micrograph of a standard gold tipping procedure on CdSe nanorods.

2.2. Methods of Characterization

2.2.1. Transmission Electron Microscopy

Introduction

When creating all new nanoscale materials, one of the greatest difficulties is clearly characterizing them. Due to the diffraction limit of light microscopes, basic imaging of nanomaterials is primarily accomplished using electron microscopes, such as a Transmission Electron Microscope (TEM). Since a TEM uses an electron beam as the light source, where glass lenses are used in an optical microscope, an electron microscope uses electrostatic and electromagnetic lenses to alter the beam[36]. When the beam passes through the nanocrystals in a TEM, the crystalline sample is likely to diffract the electron beam due to Bragg scattering. Additionally, atomically heavier and thicker samples will have greater inelastic scattering and thus lower transmittance. After the beam passes through the sample, either the resulting contrast image or diffraction pattern may be observed on a fluorescent viewing screen or detector for sample characterization. In the low resolution image, the contrast will arise from the amplitude of the zero beam that is transmitted through the sample after the scattering events mentioned above.

In addition to this basic imaging technique that will give you information on the material's shape and size, High Resolution Transmission Electron Microscopy (HRTEM) can also give you information on the crystalline packing of the nanocrystal[36]. In this technique, the contrast of the image emerges from the interaction of the phases of the transmitted and diffracted electron beams, rather than the amplitudes. By observing the

interference of the electron beams, a pattern is projected that can correspond to the packing of the crystal[37]. The trick to this method is in the interpretation. If the sample is too thick, or one's focus is off, the resulting pattern may not be interpretable without additional matching simulations[37, 38]. The problem lies in that the image does not correspond directly to the position of the atoms in the crystal, but is rather described by the contrast transfer function[36]. Even without knowing the exact position of each atom though, HRTEM can still be used to evaluate the quality of a crystal and the presence of certain defects such as stacking faults or twinning[38-40]. Figure 6, is a high resolution transmission electron micrograph taken of a batch of standard CdSe nanorods. From this image viewing down the [010] zone axis of the central rods, it is possible to make out the zig-zag wurzite structure, along with the presence of stacking faults[10, 37].

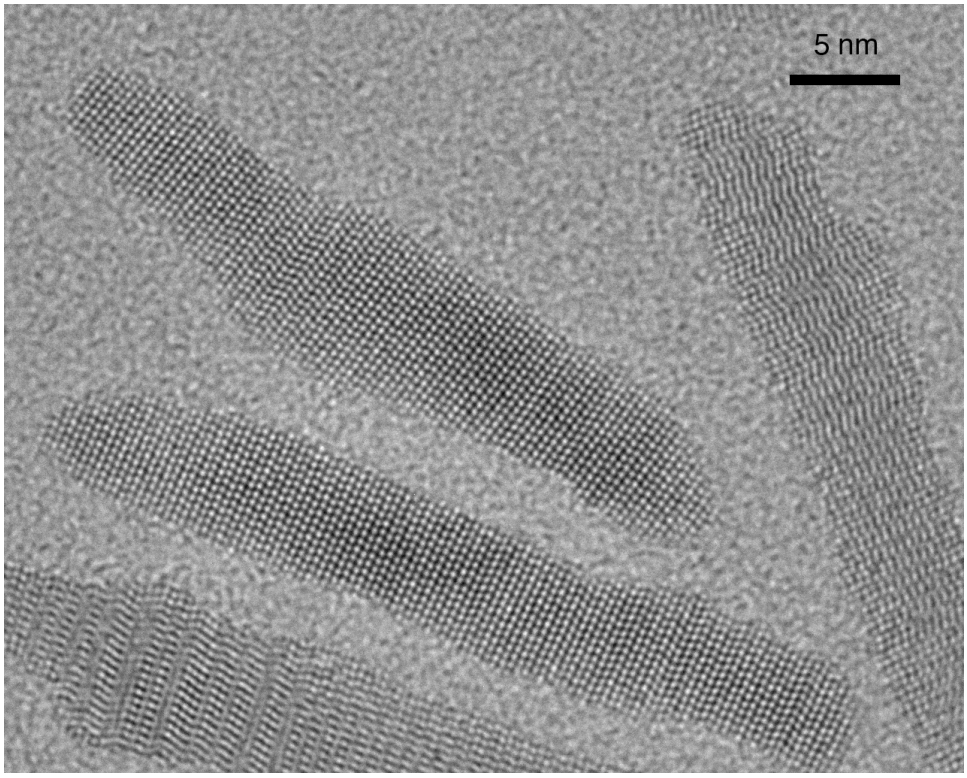

Figure 6. A high resolution phase contrast image of several CdSe nanorods, looking down the [010] zone axis. Viewed this way, the zig-zag nature of the wurtzite crystal packing may be observed as well as the presence of any stacking faults along the long c-axis.

Instrument and preparation

An FEI Tecnai G2-20 microscope was used for basic shape and size characterization along with analysis of atomic stacking. The 200 keV microscope employs a LaB6 filament and S-TWIN objective, to obtain a possible 0.14 nm line resolution or 0.24 nm point resolution. For imaging an AMT ER-B, bottom mounted, one megapixel CCD camera was used. Samples were prepared on carbon coated 400 mesh grids. For basic shape and size measurements 20-50 nm thick carbon grids were used. For High Resolution Transmission Electron Microscopy (HRTEM), Ultrathin carbon, 2-5 nm thick, grids were used. The grids were slowly dipped (2 s) in a dilute solution of nanocrystals in toluene or chloroform, and allowed to air dry. During TEM inspection multiple grid squares were inspect to insure sample uniformity. On a typical sample, 10-50 images were obtained. For HRTEM, the objective aperture was removed and a magnification of 590k was typically used. Because of the density of the samples, crystals that were lying along a zone axis were found by eye and a fair dose of patience.

2.2.2. X-ray Electron Dispersive Spectroscopy

X-ray electron dispersive spectroscopy (EDS), is a technique used to determine local elemental composition in conjunction with electron microscopes[29]. For this technique an X-ray detector is mounted on the TEM in close proximity to the sample. When the high energy electron beam passes through the sample, some of the incident electrons lose energy by ejecting inner shell electrons from the atoms in the nanocrystals.

After the loss of these inner shell electrons, an electron from a higher energy shell will drop down to fill the vacancy. During this transition, the excess energy is released as an x-ray with an energy characteristic to that particular transition. By measuring the released x-ray, elemental information can be determined about the site where the electron beam was currently probing. For this reason it is beneficial to use a scanning instrument such as a Scanning Transmission Electron Microscope (STEM) or Scanning Electron Microscope (SEM). In both of these cases, the electron beam is focused down to an area less than a nanometer in size and rasterred across the sample surface to produce an image. When elemental information is desired, the beam can be stopped temporarily to probe an area. This way, very local information can be obtained on the composition of a nanoparticle in a generally nondestructive manner. EDS spectra were collected on a Philips CM200FEG STEM with a 0.5 nm spot size. Samples were prepared the same as for basic HRTEM.

2.2.3. Optical Characterization

Optical methods have long been used a means to characterize nanomaterials because of their bandgap shifts[41-43]. The two primary methods used here are ultraviolet/visible absorption (UV/Vis) and photoluminescence emission (PL). These two methods go hand in hand as one measures the wavelength of light that the nanoparticles absorb, and the second measures the wavelength of light the particles subsequently emit. As was mentioned earlier in the introduction, because the size of these particles is on the order of the electron's bohr radius, it is possible to confine the exciton to different degrees by changing the size of the particles. As the particle is grown to smaller sizes the

confinement increases on the exciton, increasing the bandgap of the material as well. In the spectra, this change appears as a shift in the exciton peak and absorption edge to higher (bluer) energies[19]. Additionally, the width of the peak can reveal the quality of the nanocrystal sample as well. A broader peak signifies that there is a larger distribution of nanoparticle sizes present, while a narrow peak suggests there is a narrow size distribution. This is very telling for spherical particles, but less so for anisotropic nanocrystals such as nanorods since only the dimension of the width is confining the exciton. Due to this fact, not as much information regarding the length of the nanorod can be gleamed from the absorption data.

If the light incident on the nanoparticle is sufficient in energy, it can excite the particle and form an electron/hole pair. When the pair recombines there will be a characteristic emission for the particle. The quantum yield of the nanoparticle's PL is an interesting piece of information, since it gives one a sense of the quality of the surface passivation of a nanoparticle[27]. If there are few surface traps and the particle is well passivated there should be a high yield and strong emission. However, if the particle is poorly passivated or if a metal is grown on the surface, the PL will be decreased or even fully quenched.

For the optical characterization, a small amount of the nanoparticles were diluted in toluene shortly after cleaning to ensure a consistent passivation. For the PL a Jobin Yvon - Spex Triax 320 spectrometer was used. While for UV/Vis a Hewlett Packard 8453 UV/Vis diode array spectrometer equipped with a deuterium lamp was used with a resolution of 1 nm.

Chapter 3. Polytypism and Stacking Fault Formation

3.1. Introduction

The ability to prepare inorganic nanocrystals with complex shapes and spatial arrangements continues to advance[3, 22, 44]. In colloidal nanocrystals, it is now well established that highly anisotropic shapes can be formed under kinetic control, where relative growth rates of different facets are manipulated[2, 4]. CdSe and CdTe wurtzite nanorods, in which ABAB planes stack rapidly along the hexagonal axis, serve as good examples[4]. In the II-VI semiconductors, wurtzite (ABAB) and zinc blende (ABCABC) stackings are both common[10, 37]. The presence of stacking faults, or ABC sequences within an otherwise hexagonal packed nanocrystal, have long been noted and investigated[39]. Recently, however, it has become clear that when controlled, this polytypism can be exploited as a means of creating branched structures, such as tetrapods, (a zinc blende core is formed, followed by the growth of four wurtzite arms), or as a means of spatially modulating the potential for electrons and holes[12, 45]. In order to achieve a higher degree of control over the growth process, it is desirable to know more about how stacking faults arise spontaneously during the growth of rods. In this work we investigate the evolution of the stacking fault distribution over time, and we show that the observed distribution can be used to better understand the growth mechanisms on these nanorods.

3.2. Experimental Methods

CdSe and CdS nanorods of different lengths were selected from standard growth reactions by removing aliquots at different times, and then the nature and location of the stacking faults in a statistically significant number of individual nanorods were observed by High Resolution Transmission Electron Microscopy (HRTEM). The primary synthesis technique used for these analyses was one using cadmium oxide complexed with alkyl-phosphonic acids for the cadmium precursor under air free conditions. The cadmium oxide was mixed in a roughly 1:2 (Cd:phosphonic acids) ratio with phosphonic acids (75% tetradecylphosphonic acid and 25% hexylphosphonic acid), and disolved in Trioctyl-phosphine oxide (TOPO) at 120 °C. The CdO dissociates around 200 °C, and the anion precursor, complexed with Trioctyl-phosphine (TOP), was injected at roughly 300 °C. The rods were grown for approximately 5 -10 minutes after anion injection. Using slight modifications of this general procedure, CdSe rods were grown with the following dimensions (nm): 49.5 +/- 6.2 nm x 6.4 +/- 0.7 nm, 31.4 +/- 5.8 x 6.2 +/- 0.6 nm, 18.7 +/- 2.2 nm x 7.0 +/- 0.7 nm, and a single synthesis of rods sampled at multiple times: 12.0 +/- 2.2 nm (3:15 min), 23.3 +/- 2.3 nm (4:45 min), and 39.3 +/- 5.0 nm (10:00 min). Cadmium sulfide rods, grown in a similar fashion,[2] were 29.1 +/- 4.1 nm long. Finally, CdSe rods grown using dimethylcadmium precursor, a commonly used technique[46], were grown to 21.2 +/- 2.4 nm long.

Stacking faults in the nanorods were observed using a 200 kV LaB_6 FEI Tecnai G^2 20 HRTEM, equipped with a Super TWIN lens. High resolution images were obtained for approximately 60 nanorods from each sample. Stacking faults consist of a certain number of zinc blende (ABCABC) layers within the larger wurtzite lattice. A complex

fault (ABABCBC) is the most commonly observed fault, with 3 layers of zinc blende. In an intrinsic fault (ABABCACA) there are 4 zinc blende layers, and in an extrinsic fault (ABABCABAB) there are 5[39]. Each of these patterns was directly observed and recorded, as demonstrated in Figure 7.

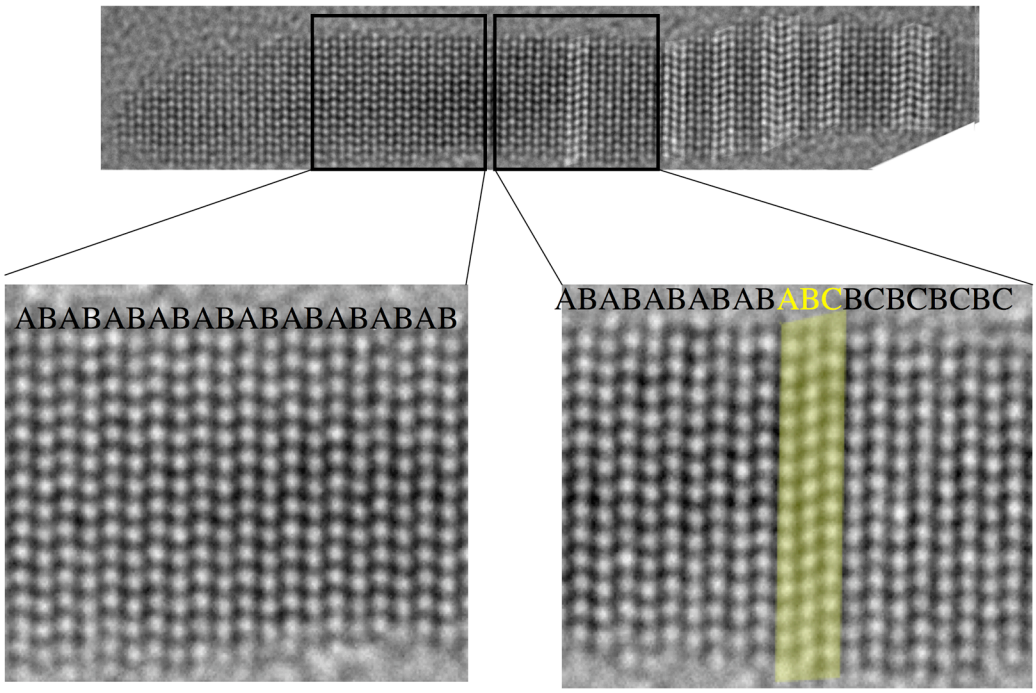

Figure 7. The above HRTEM image shows how stacking faults were identified and counted in a typical sample. In this case the faults would be measured starting from the right since that end has the higher concentration of faults. The boxed region on the left is blown up from a region with no faults. One can see the repeated ABAB pattern of the wurzite packing. The blown up region on the right however, contains a complex fault as shown by the shift due to the insertion of the C layer.

3.3. Varying Rod Length

3.3.1. Experiment and Results

The average number of faults per rod ranged from 2 for the 12.0 nm long rods, to 10 for the 39.3 nm long rods. Remarkably, we found that the positions of the stacking faults in the nanorods were not uniformly distributed. A clearly anisotropic distribution of faults along the length of the rods was observed, as shown in Figure 8. Here three different lengths of rod were observed, all with approximately the same 7 nm width. The exact position of each fault was recorded in the 19, 31, and 50 nm rods, and while the number of faults and their precise locations change for each individual rod, shown in the left plot, the region in which they form remains a fixed percent of the rods length, right plot. Measurements were taken from the end with the highest density of faults for consistency. In the case of these rods, that region is approximately 40% of the rod measured from an end, regardless of the rod's size.

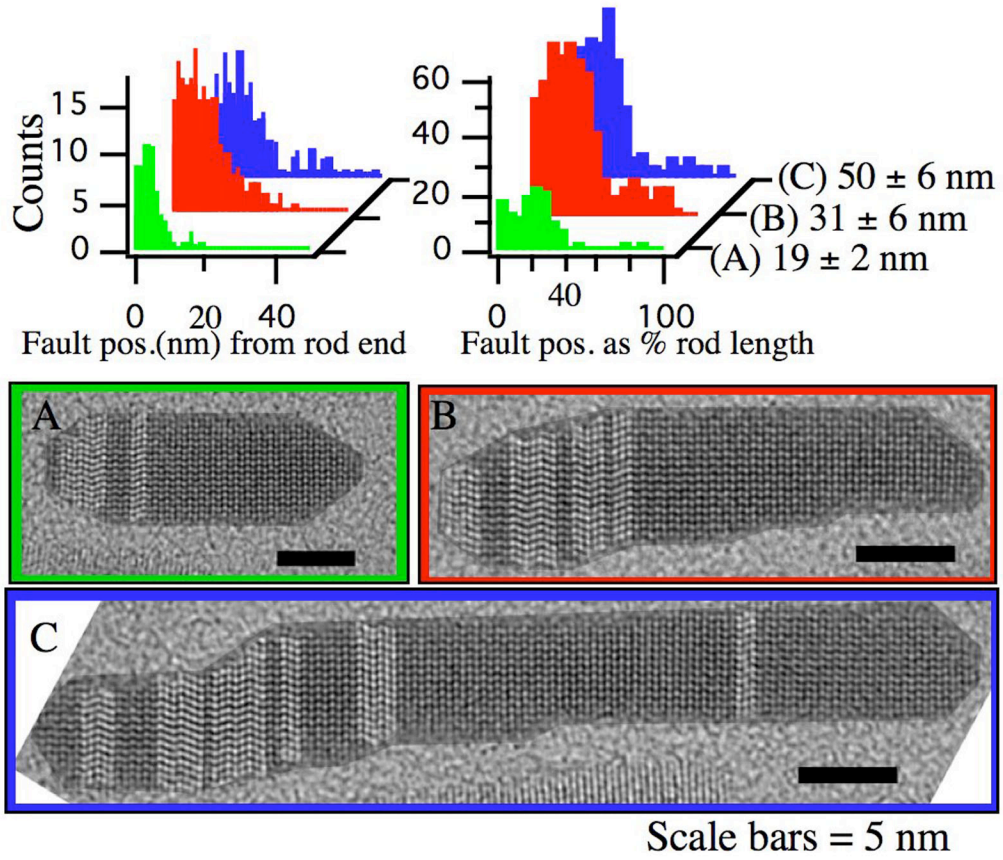

Figure 8. Statistics taken from 19, 31, and 50 nm rods. Left plot contains histograms of actual stacking fault positions as measured from the end of the rod with higher fault density. The right plot histograms are the same fault position data normalized as a percent of the individual rod lengths.

3.3.2. Discussion

This anisotropic distribution of stacking faults is consistent with prior thinking about the mechanism of growth of anisotropic colloidal CdSe nanocrystals. Rapid growth occurs along the c-axis of the CdSe[4], but it is very important to realize that the two ends of the rod are not equivalent. There is no inversion symmetry along this axis, and the faces at either end of the rod are chemically distinct. If unreconstructed and not ligated, the cadmium atoms on the (001) face would have a single dangling bond, while the cadmium atoms on the (00-1) face would have three dangling bonds. Theoretical studies have shown that the phosphonic acid ligand binding strength on these surfaces is different, consistent with a model in which the ligand coverage during growth on the two faces are not the same. While both of these polar faces are likely less well passivated than the nonpolar sides of the rod, the (00-1) face likely has the lowest coverage[47]. Because of this anisotropy, the (001) face is considered the slow growing face, while the (00-1) is the fast growing face and is likely the location for the majority of the rod's growth[1]. Additionally, the +/-(001) faces of wurtzite epitaxially match the four equivalent (111) faces of zinc blende[12]. Thus, a simple hypothesis to explain the observed fault distribution is that stacking faults are prefentially formed on the (001) face.

3.4. Stacking Fault Growth Evolution

3.4.1. Experiment and results

This hypothesis can be tested by examining how the distribution of stacking faults changes during growth. For this experiment a sample was analyzed at multiple points in time throughout its growth, Figure 9. During the time series shown here the rod grows from 14.8 nm +/- 1.7 nm sampled at 3:15 min, to 23.7 nm +/- 2.4 nm at 4:45 min, and ending at 42.9 nm +/- 4.3 nm after 10:00 min. As the growth continues the statistics show that faults continue to form as well throughout the synthesis, increasing from an average of 2 faults/rod to 4 faults/rod, and ending at approximately 10 faults/rod. The distribution meanwhile, appears to stabilize at a 40/60 split between the growth regions after an initial increase between the first two sampled periods.

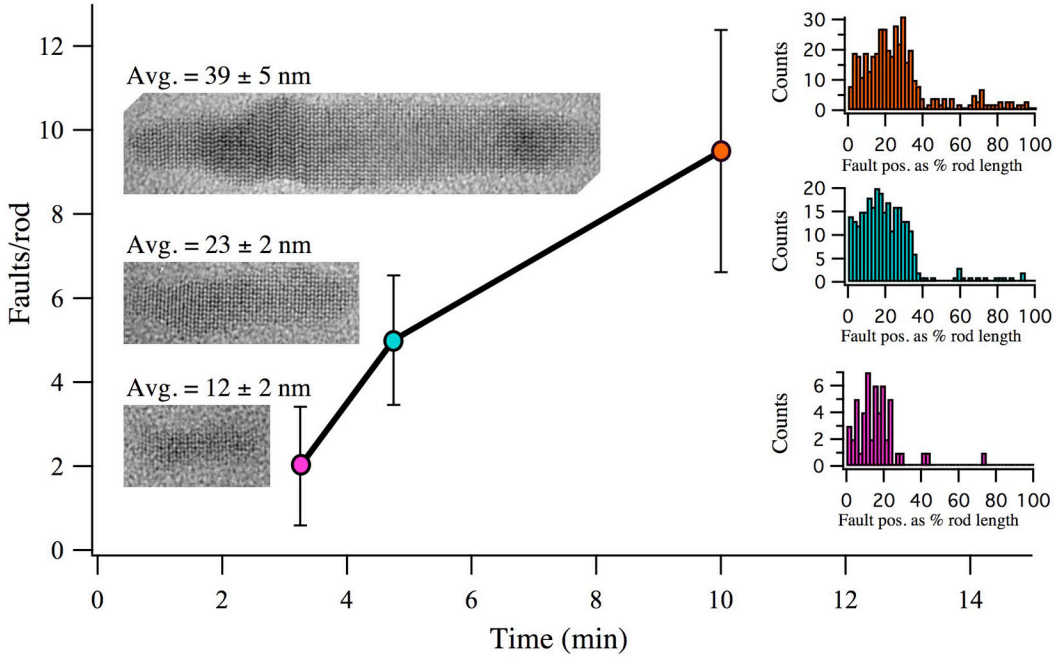

Figure 9. In the single growth experiment above, as the rods mature more faults continue to form. Aliquots were taken and characterized at 12, 23, and 39 nm. At 12 nm, there is an average of 2 faults/rod, at 23 nm there are 5 faults/rod, and finally at 39 nm there are 9 faults/rod. Additionally, the shape of the distribution of faults in the rods remains consistent as shown in the histograms on the right.

3.4.2. Discussion

For this distribution to be maintained, the faults must continue to form throughout the rod's growth at a fixed rate on a particular face. Consequently, the rod may be characterized as comprising of two different regions: one fault rich, and one mostly fault free. By inference, the smaller region containing the faults can be attributed to the slow growing (001) face, while the larger fault free region is thus due to the fast growing (00-1) face. Figure 10 completes the picture of the growth of a CdSe rod. The growth is broken down into two fronts shortly after nucleation. The (00-1) face, with its poor ligand coverage of the three dangling cadmium bonds, grows fast and with few faults. Meanwhile the greater passivation of the (001) face likely forms a kinetic barrier, resulting in slower growth and numerous stacking faults. Interestingly, the separation between the growth rates of these two faces is actually smaller than previously believed; with a ratio of 2:3, the slow growing (001) face accounts for a considerable portion of the rod's makeup.

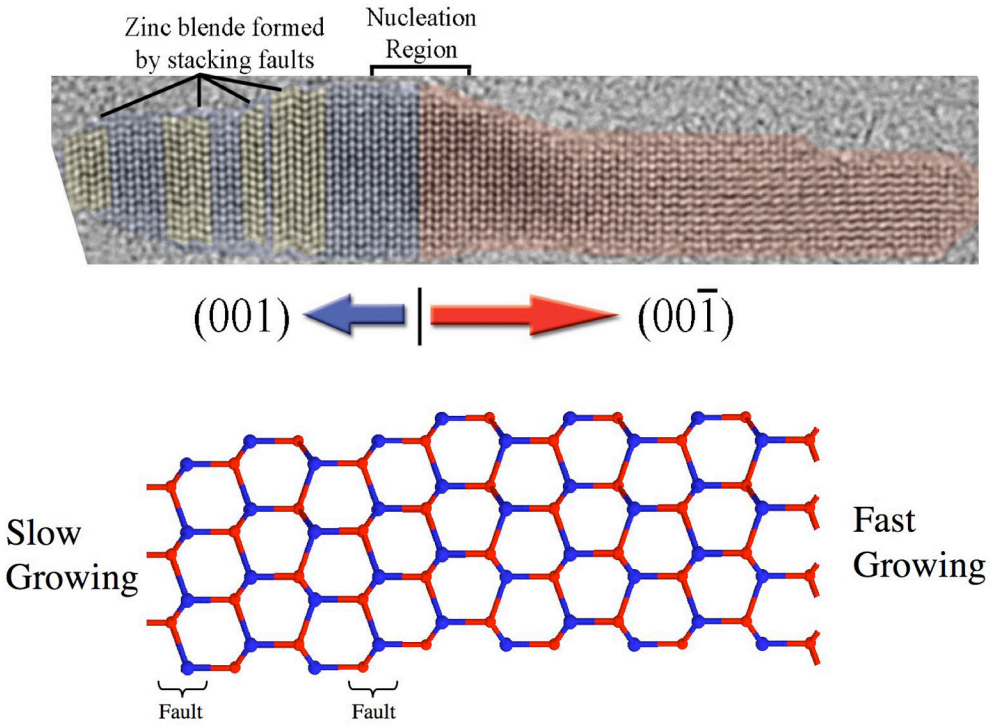

Figure 10. The above model for rod growth has the rod split into two regions of growth after an initial nucleation event. The growth from the (00-1) face, red, with three dangling cadmium bonds, is fast and mostly fault free. The growth in the opposite direction from the (001) face, blue, with one dangling cadmium bond, is slower and highly faulted. The faults in the slow growing region have been highlighted in yellow.

3.5. Generality

3.5.1. Experiment and Results

Two additional systems were analyzed as well to determine whether this behavior was a unique or more general phenomenon. The first was CdSe rods grown using dimethyl cadmium as the cadmium precursor instead of using the afore mentioned technique with cadmium oxide[46]. Using the same analysis procedures, in a sample of 29 x 6 nm rods there is an average of 3 faults/rod, which are in a region accounting for only 20 % of the rod's length. Compared with 9 faults/rod in the 31 nm long rods from Figure 8, one can see why it may be that these rods are preferred for experiments that require a higher quality such as alignment in liquid crystals[35]. This anisotropic distribution, though, does not appear to be isolated to CdSe. Cadmium sulfide rods grown by a technique similar to the method outlined earlier exhibit the behavior as well. For a batch of 29.1 +/- 4.1 nm rods, there were an average of 3 faults/rod typically confined in a region of 20 % of the rod's length. With so few stacking faults these CdS rods are more similar to the CdSe rods grown using dimethylcadmium.

3.5.2. Discussion

These results suggest that the anisotropic fault distribution may be a more generalized phenomenon which can be observed in other II/VI semiconductor nanomaterials as well as those observed in this study. Additionally, while the behavior is apparent in all these cases, the degree of anisotropy does change, and ultimately affect the

quality of the rods. This is because any change in the rod growth kinetics, and the ratio of the growth rates between the (001) and (00-1) faces, will change the relative size of the fault region. Thus by decreasing the size of this fault region more defect free rods may be grown.

3.6. Conclusions

These findings give new insight to the growth mechanism of nanocrystals, and a new means to easily characterize nanorods in more complex systems. The results suggest that the slow growing face contributes more to the size and quality of the rod than previously thought. The degree of this contribution may be controlled to form higher quality rods by altering the synthetic technique to decrease the contribution of the faulty, slow growing crystal face. A further understanding of the mechanism of stacking fault formation may help us understand how better to control the quality and possibly the branching of nanocrystals in the future. As a means of nanostructure characterization, this technique is a simple means to qualitatively identify the orientation of the nanorod's growth in more complex structures by identifying the end with the greater density of stacking faults.

Chapter 4. Heterostructures

4.1. Introduction

The development of colloidal quantum dots has led to practical applications of quantum confinement, such as in solution processed solar cells[48], lasers[49] and as biological labels[29]. Further scientific and technological advances should be achievable if these colloidal quantum systems could be electronically coupled in a general way. For example, this was the case when it became possible to couple solid-state embedded quantum dots into quantum dot molecules[50, 51]. Similarly, the preparation of nanowires with linear alternating compositions—another form of coupled quantum dots—has led to the rapid development of single-nanowire light-emitting diodes[52] and single-electron transistors[34]. Current strategies to connect colloidal quantum dots use organic coupling agents[53, 54], which suffer from limited control over coupling parameters and over the geometry and complexity of assemblies. Here we demonstrate a general approach for fabricating inorganically coupled colloidal quantum dots and rods, connected epitaxially at branched and linear junctions within single nanocrystals. We achieve control over branching and composition throughout the growth of nanocrystal heterostructures to independently tune the properties of each component and the nature of their interactions. Distinct dots and rods are coupled through potential barriers of tuneable height and width, and arranged in three-dimensional space at well-defined angles and distances. Such control allows investigation of potential applications ranging from quantum information

processing to artificial photosynthesis.

4.2. Heterostructure Background

Unlike VLS– or SLS–grown nanowires, anisotropic nanocrystals in homogeneous solutions grow without the benefit of catalyst activation of one end. Hence, heterostructure growth in colloidal nanocrystals has so far been limited to core/shell structures that serve primarily to further isolate quantum dots from their environment[18, 55-58]. An elegant extension of core/shell growth enabled concentric alternating layers of CdS and HgS, which have a Type I (nested) band alignment[59, 60]. Control over the electronic structure of concentric heterostructures is, however, restricted by their simple geometry and by strain due to lattice mismatch, which typically limits the thickness of each layer to a few monolayers or less. Heterostructures based on nanorods permit more complexity and their properties are fully tuneable since strain does not limit their dimensions.

Anisotropic colloidal heterostructures are fabricated by sequential growth of semiconductor dots and rods of different materials, with the possibility for branched connectivity in each generation. Branching is introduced through crystal phase control[2, 3, 12], so the large class of semiconductors exhibiting zinc blende–wurtzite polytypism[10] could be incorporated into branched heterostructures by these methods. Recently, limited phase control enabled the high yield synthesis of tetrapod shaped nanocrystals of a single material, CdTe[12], effectively arranging four quantum rods of the same composition around a central dot. This fundamental branched structure results from nucleation in the cubic zinc blende phase with subsequent anisotropic growth in the hexagonal wurtzite

phase. Here, we demonstrate that branched and linear junctions can be created not just at nucleation, but at any point during the growth of heterostructures. Considering two generations of growth within this paradigm, four basic structures can be postulated and were synthesized. The first generation nanostructures can be linear, wurtzite rods, or branched tetrapods. On these two basic structures, a second material is grown in either branched or linear fashion as shown in Figures 11 and 12. The dimensions of each generation define the degree of quantum confinement and are controlled by methods developed for nanorod growth[1]. The terminal rods and dots are coupled through the tuneable barrier defined by the first generation, while more generations of growth would produce structures incorporating even more complex interactions. In a preliminary exploration of novel properties of nanocrystal heterostructures, long–range photoinduced charge separation has been achieved in Type II (staggered band) heterostructures, evidenced by the quenching of nanocrystal luminescence. Type I heterostructures permit tuneable exchange coupling between the terminal quantum dots or rods.

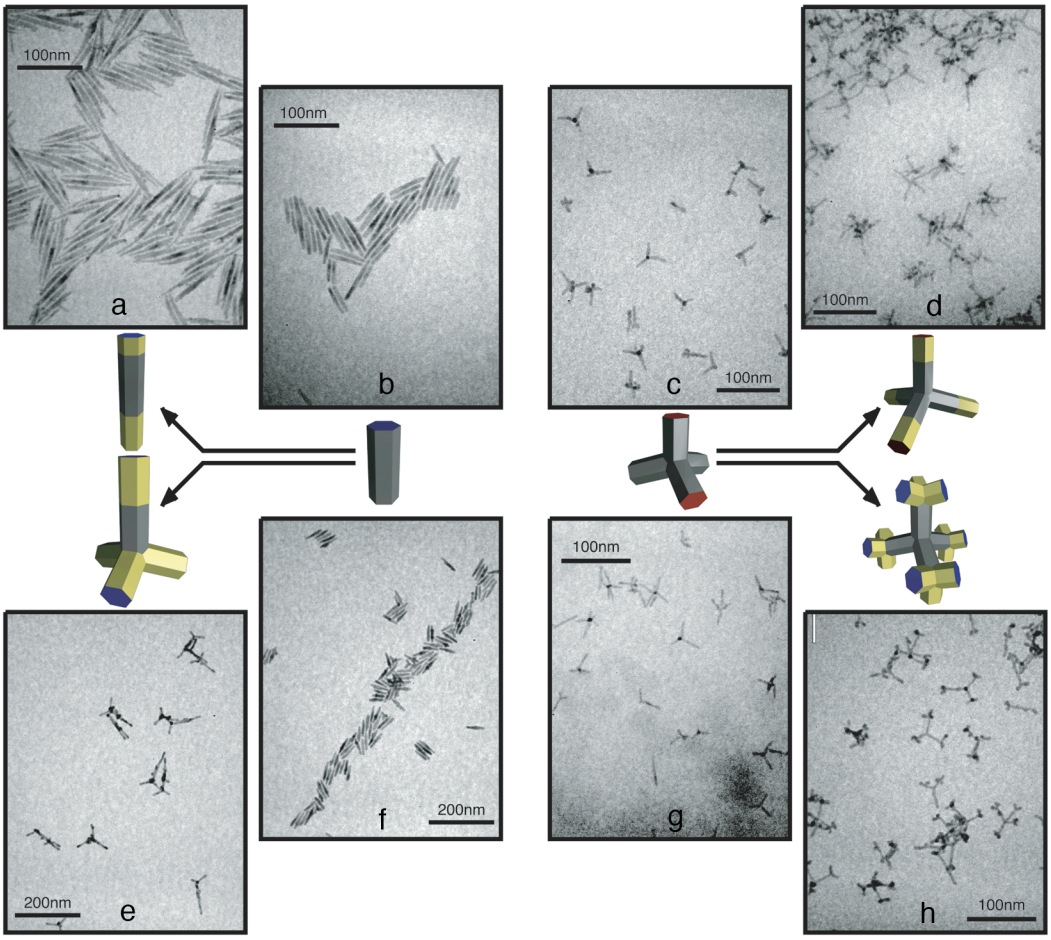

Figure 11. A survey of the possible nanocrystal heterostructures shown with graphical models and real micrographs obtained after growth experiments. Extended rods (a) were formed by first growing CdS nanorods (b), then adding CdSe extensions to each end. Branched rods (e) result from nucleating CdTe on either end of the original CdSe nanorods (f). One end nucleates the CdTe in zinc blende resulting in a branch point. CdSe tetrapods (c, g) can have either linear extensions of CdTe grown at the ends of each arm (d) or branch points formed by zinc blende nucleating at the ends of the arms (h).

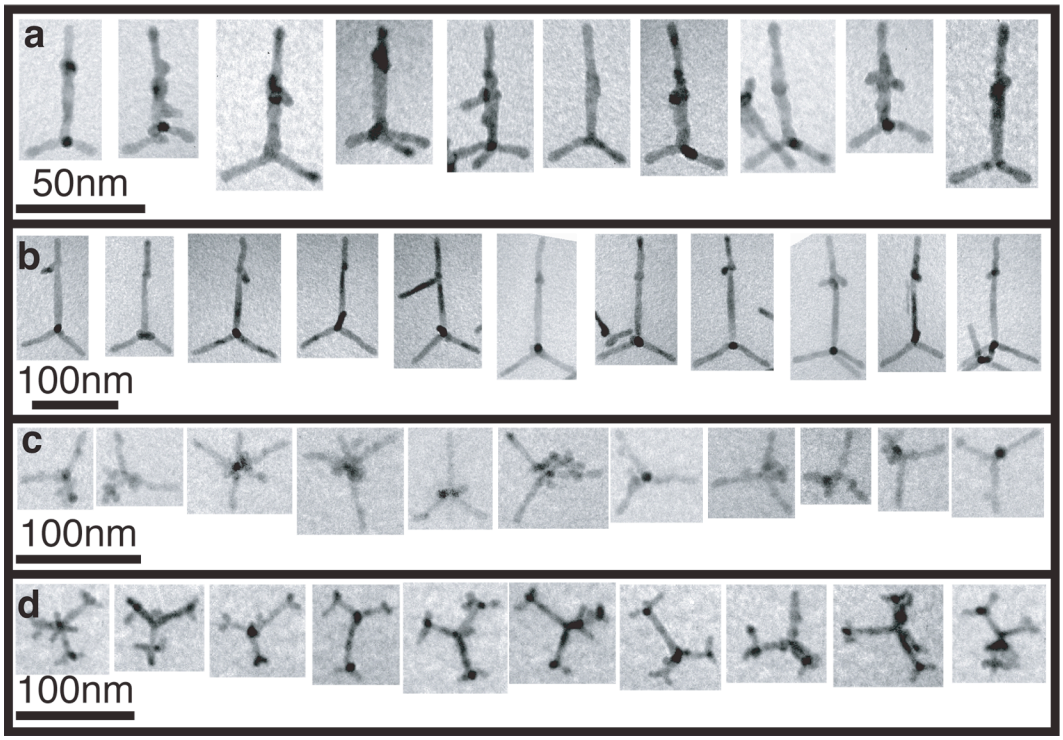

Figure 12. A closer look at nanocrystal heterostructures. The isolated particles allow examination of structural aspects such as 'back branching' in branched rods (a and b) and extended tetrapods (c) and structural isomers in branched tetrapods (d). Branches projecting from the linear junction at an angle back along the original rod arise in regions containing many stacking faults at the heterojunction and are consistent with the symmetry relationships between the zinc blende and wurtzite phases. Secondary branches in branched tetrapods (d) grow either staggered or eclipsed with respect to the arms of the original tetrapod. Heterostructures in a, c and d are CdTe grown on CdSe, and in b are CdTe grown on CdS.

4.3. Synthetic Methods

New methods were developed to grow a second material selectively on the ends of nanorods and to create branch points at will. Unlike core/shell nanocrystals, heterostructures were grown in the kinetic control regime previously exploited for CdSe nanocrystal shape control[3]. First generation structures were grown by modifications of previously reported methods for preparing elongated nanocrystals[1-3, 12]. In all cases, cadmium oxide complexed by alkylphosphonic acids was used as the cation precursor[2]. The anion precursor (elemental Se, S, or Te dissolved in tri(n-alkylphosphine)) was injected at a temperature between 280 and 320 ºC to initiate growth. Linear heterojunctions were formed when precursors for a second material were added to a growth solution containing preformed nanorods or tetrapods. Branched junctions were introduced preferentially at high supersaturation of these precursors. The second generation was typically grown without isolation of the nanocrystals by using an excess of cadmium in the first step and injecting the anion precursor for the second material. Thus, in this work, all the reported heterostructures have cadmium as a common cation. Linearly extended rods were synthesized with CdS rods and CdSe extensions, while the other structures were synthesized with CdSe in the first and CdTe in the second generation. Branched rods were also synthesized with CdS rods and CdTe branches. All of the heterostructures could be readily dispersed in common organic solvents, such as toluene and chloroform, and were prepared in high yield without any post–synthetic separation. Similar results were achieved by isolation of the first generation nanocrystals

and reintroduction of cadmium precursor prior to injecting the second anion precursor, implying extensibility to heterostructures incorporating semiconductors that do not share common ions.

Reversing the growth sequence under similar synthetic conditions changed the growth pattern of the second material from selective on the ends to more homogeneous core/shell growth. For example, growing CdTe followed by CdSe, we succeeded in synthesizing Type II core/shell tetrapods, Figure 13. As observed previously for core/shell nanorods[46], elongated growth from the ends of core/shell tetrapods proceeds only after several monolayers of shell have formed and strain limits further homogeneous growth. In contrast, in branched and linear heterostructures, we suggest that the difference in surface energy between two materials favours end selective growth. Although in principle, they limit materials selection for a given topology, these observations suggest that any pair of materials in this class[10] could be combined in core-shell or in end-selective structures by reversing their growth order.

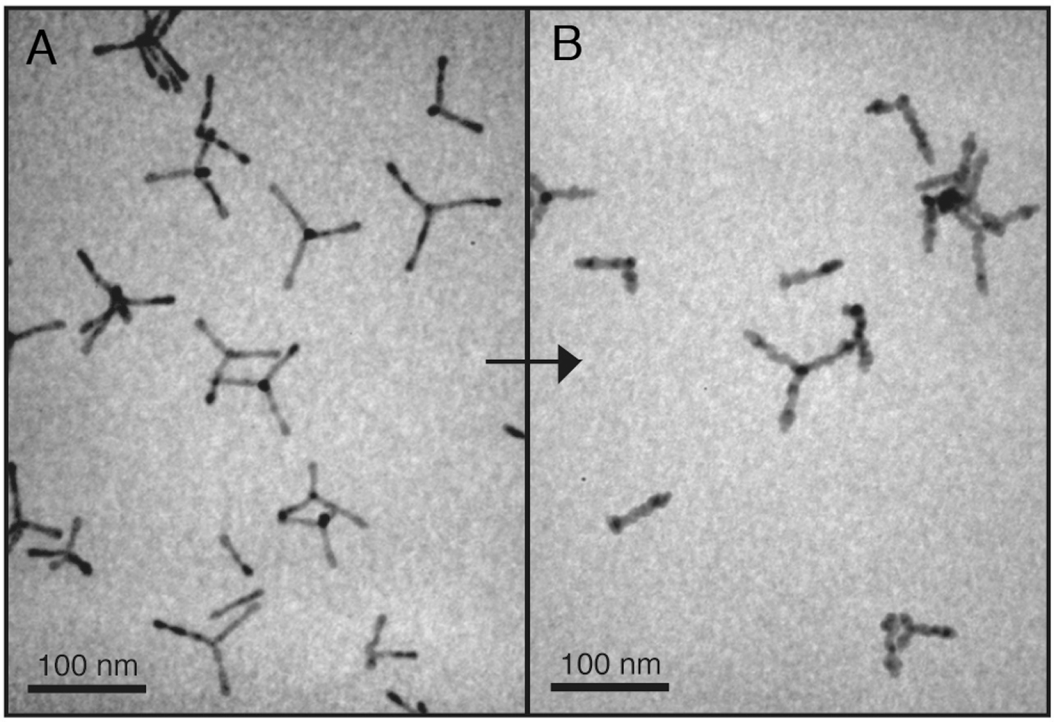

Figure 13. CdTe tetrapods with a CdSe shell grown on them in a subsequent anion addition. The order in which the anions were injected for growth determines whether the final structures will be core/shell nanocrystals such as here, or heterostructures.

4.4. Characterization

4.4.1. EDS

Several techniques were applied to establish the end selectivity of heteroepitaxy in these nanocrystal structures. Nanoprobe x-ray energy dispersive spectrometry (EDS) was used to examine the local atomic composition of the heterostructures[29]. Resulting EDS line scans shown in Figure 14 confirm the presence of Te at either end of branched rod heterostructures, Se in the central rod, and Cd throughout. The remnant tellurium signal in the middle section results from partial overlap with an adjacent Cd peak and is observed in similar magnitude in CdSe nanorods containing no Te. Results on extended rods, Figure 15, similarly confirm end long growth of thinner CdSe extensions on CdS rods. While a sufficiently small spot size was used, the spatial resolution of the EDS data was limited by the drift of the instrument so that it remains uncertain how compositionally abrupt the interfaces are. The apparently few-nanometer width of the compositioin gradient is an upper bound. To see more clearly whether the end long growth is accompanied by the formation of a thin shell, the powder x-ray diffraction patterns at different stages of growth were examined, Figure 16. While significant peak shifts due to strain result from the growth of shells even one monolayer thick on nanorods[46, 61], we observed no obvious peak shifts in the case where growth occurs on the ends only.

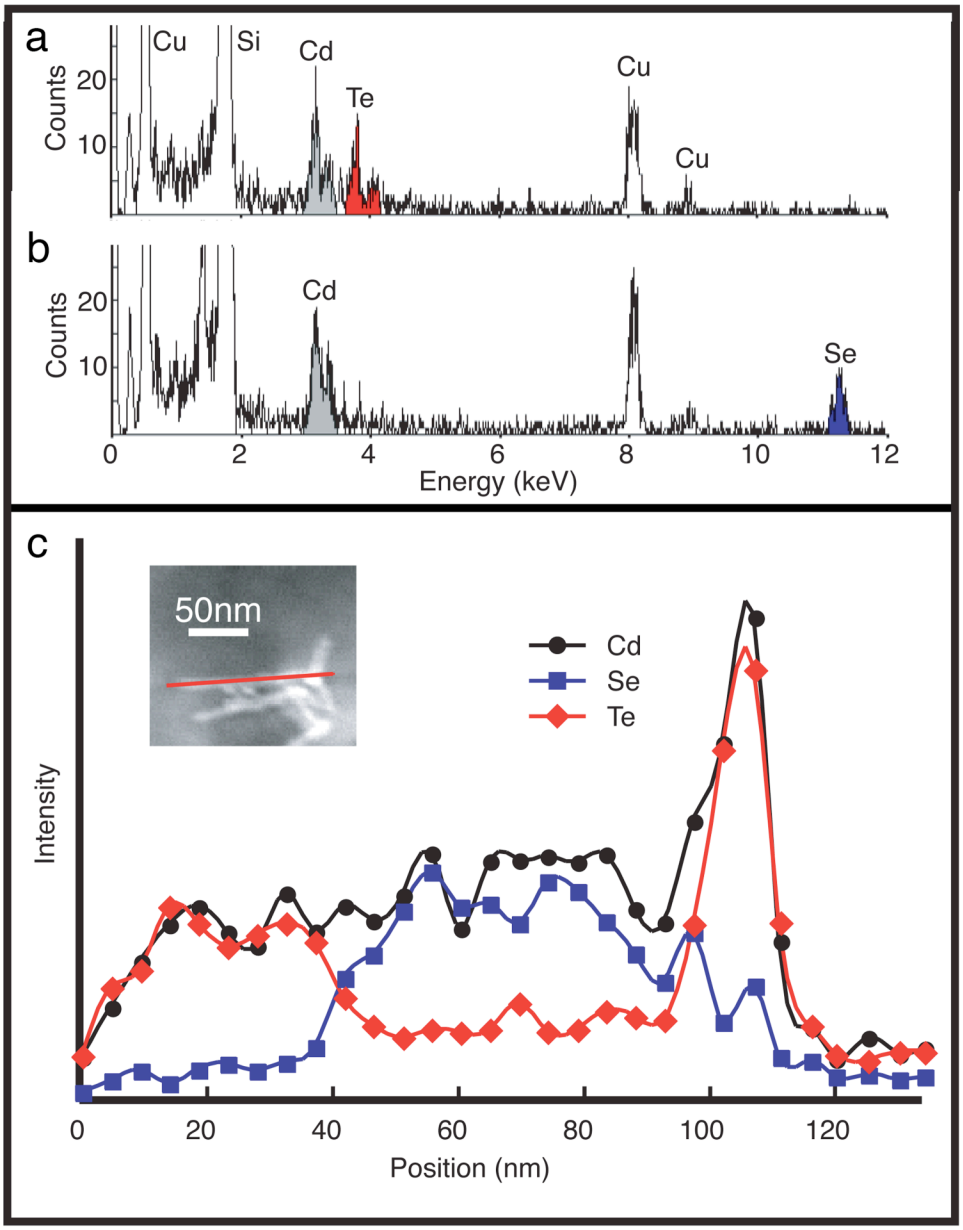

Figure 14. Analytical electron microscopy of a heterostructure nanocrystal. Representative spectra from the CdTe portion (a) and CdSe portion (b) of the heterostructure inset in (c), a nanoprobe EDS line scan along a branched rod. The line scan confirms CdTe growth on CdSe. The high intensity spike corresponds to the CdTe arm projecting out of the plane from the branch point.

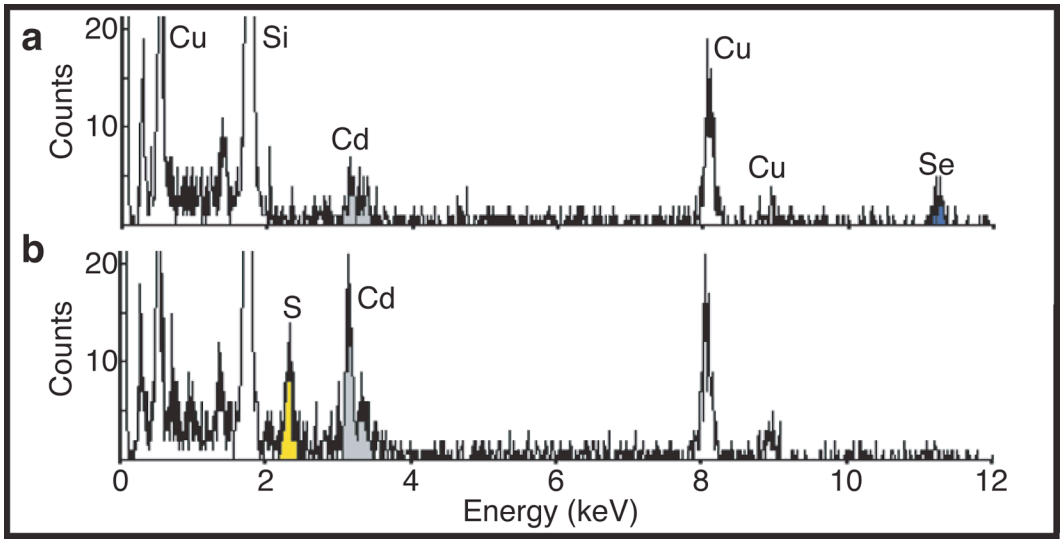

Figure 15. Representative EDS spectra from a CdS/CdSe extended rod. Top spectrum (a) shows the presence of the Se peak, while the bottom spectrum (b) shows the sulfur peak just below the cadmium signal, and no selenium peak.

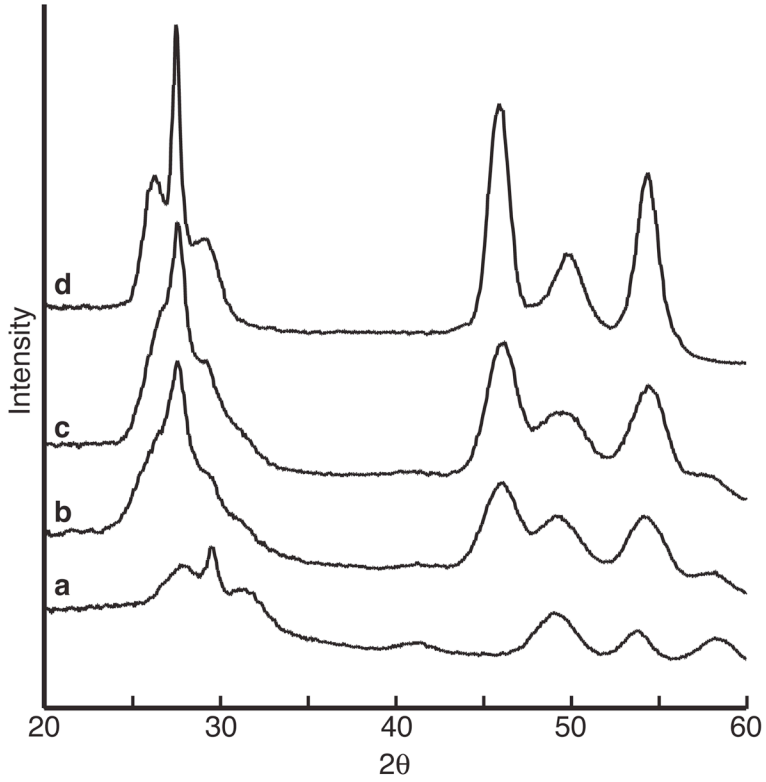

Figure 16. X-ray diffraction patterns of branched rod heterostructures. CdTe was grown onto CdSe (a) nanorods. As the CdTe grew (b and c), characteristic peakes rapidly appear in the pattern. The XRD pattern of CdTe tetrapods (d) is provided as a reference.

4.4.2. TEM statistics

Furthermore, statistical length and diameter distributions extracted from TEM images, Figure 17, indicate no significant change in diameter upon growth of the second material. For example, the radii of the arms of one batch of CdSe tetrapods were 2.9±0.4 nm before growing CdTe extensions, and 2.9±0.5 nm afterwards. CdS nanorod radii were 3.6±0.4 nm before and 3.9±0.5 nm after growing CdSe extensions where, due to the tapered shapes of the CdS rods and of the heterostructures, the radius is taken as the maximum. The small increase in radius is consistent with the formation of at most one monolayer of CdSe on the sides of the CdS nanorods.

4.4.3. Optical

Finally, while several of these heterostructures are Type II, their optical absorption spectra lack distinctive sub-band gap tails like those observed for Type II core/shell quantum dots[58] and for our core/shell tetrapods, Figure 18. Due to the very small scale of these heterostructures, no technique allows us to eliminate the possibility that a very thin (one monolayer) shell grows by overgrowth or ion exchange, however, taken together, these results strongly indicate selective heteroepitaxial growth on the ends of nanorods and tetrapods.

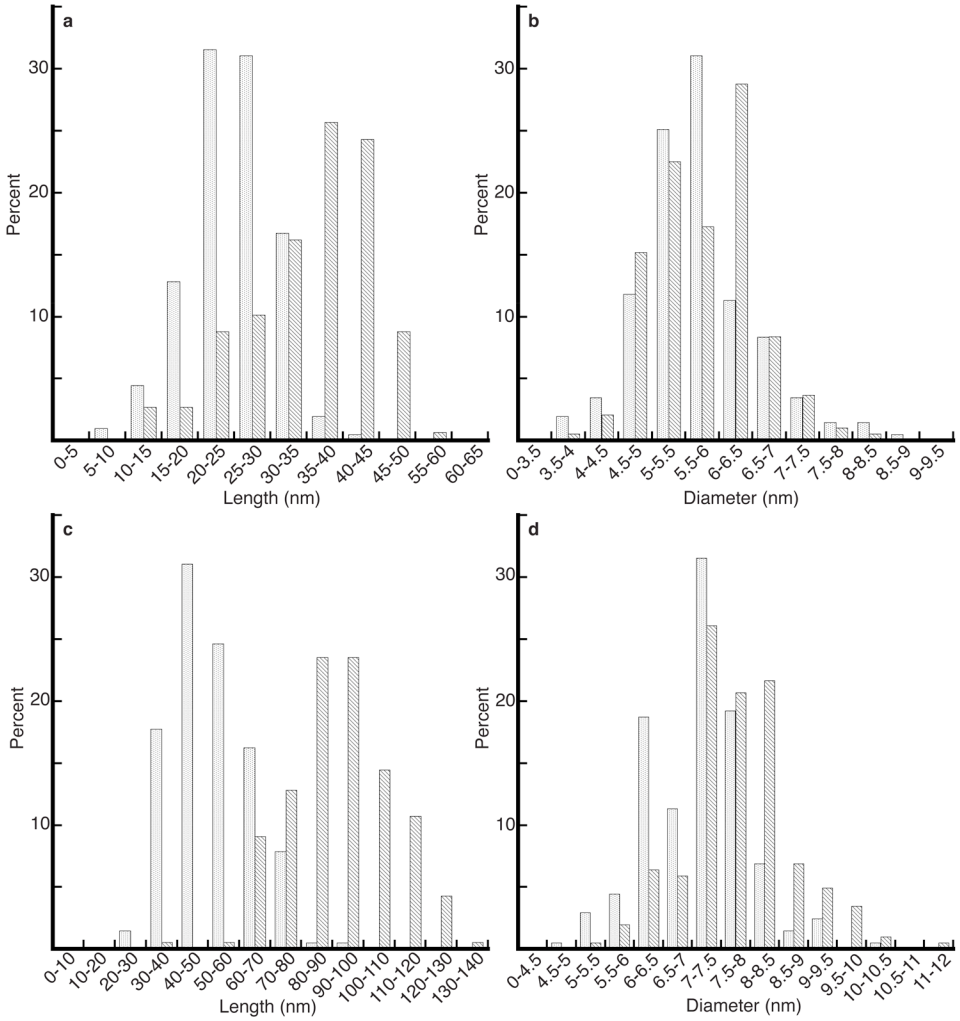

Figure 17. The length (a) and diameter (b) are compared for CdSe tetrapods before and after extending the arms with CdTe. The arms of CdSe tetrapods lengthen from 24 +/- 6 nm to 35 +/- 8 nm with the addition of CdTe. Length (c) and diameter (d) of CdS rods are compared before and after adding CdSe extensions. CdS rods increase from 52 +/- 13 nm to 92 +/- 17 nm upon growth of CdSe extensions.

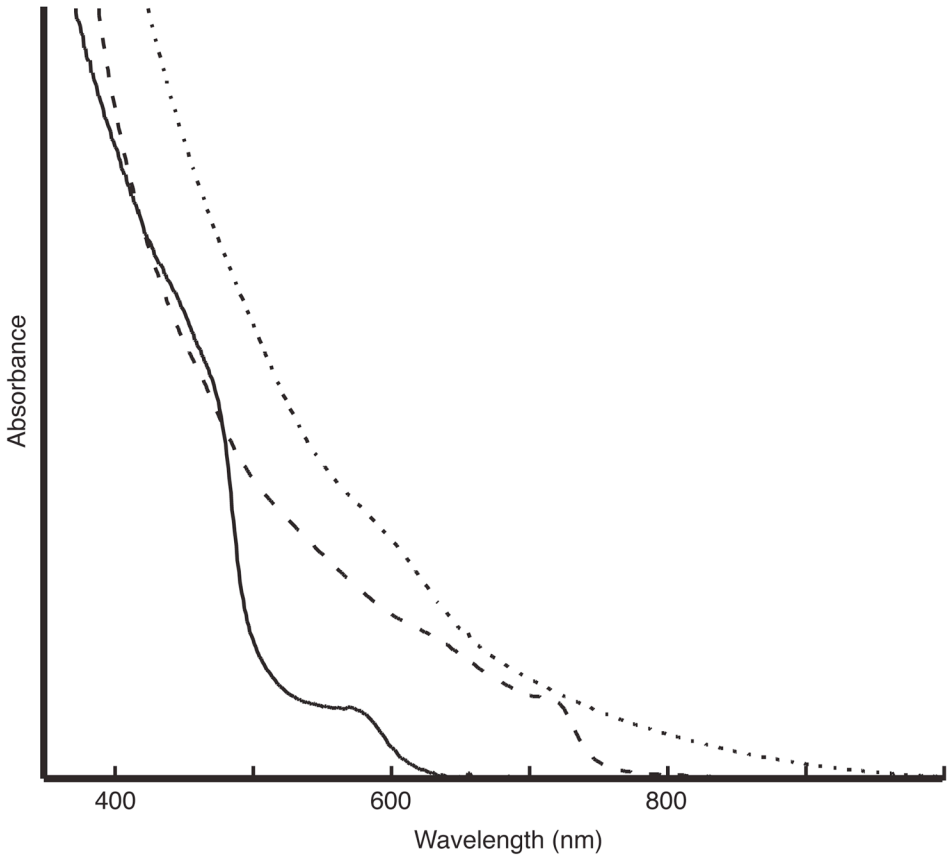

Figure 18. Optical absorption spectra of representative heterostructures. The absorption spectra for CdS/CdSe extended rods, solid, and CdSe/CdTe branched rods, dashed, show features above the bandgap of each component material, characteristic of all the extended heterostructures. Well-dispersed core/shell CdTe/CdSe tetrapods, however, exhibit a distinctive sub-band gap tail, dotted, not found in any of the extended heterostructures.

4.4.4. HRTEM

The topology of each generation is determined by the initial growth phase of the nucleating material. Nanorods and tetrapod arms grow in the wurtzite structure, elongated along the unique c-axis. Invariably, such nanocrystals contain a statistical distribution of stacking faults which convert the growth to zinc blende and back to wurtzite along the rod, sometimes leading to kinks or other irregularities[1]. High resolution transmission electron microscopy (HRTEM) of linear junctions found in extended rods and tetrapods, and in branched rods, reveals a continuation of anisotropic wurtzite growth in the second semiconductor, Figure 19, often accompanied by a high concentration of stacking faults. At these junctions, the small diameter allows dislocation free epitaxial growth despite fairly large lattice mismatches. The heterostructures with the largest mismatch (CdS/CdTe) accommodated an 11% mismatch easily, Figure 19. In HRTEM, branch points could most easily be observed by imaging branched rods that were missing one of the three CdTe branches, Figure 19. In such nanocrystals, a well formed CdTe zinc blende region could be seen at the junction. Thus, a branched junction forms when the new material initially grows in the zinc blende structure, followed by a reversion to anisotropic wurtzite growth, forming the branches. Zinc blende formation is favoured by a high supersaturation of the precursors immediately following injection, with wurtzite growth resuming as concentrations drop.

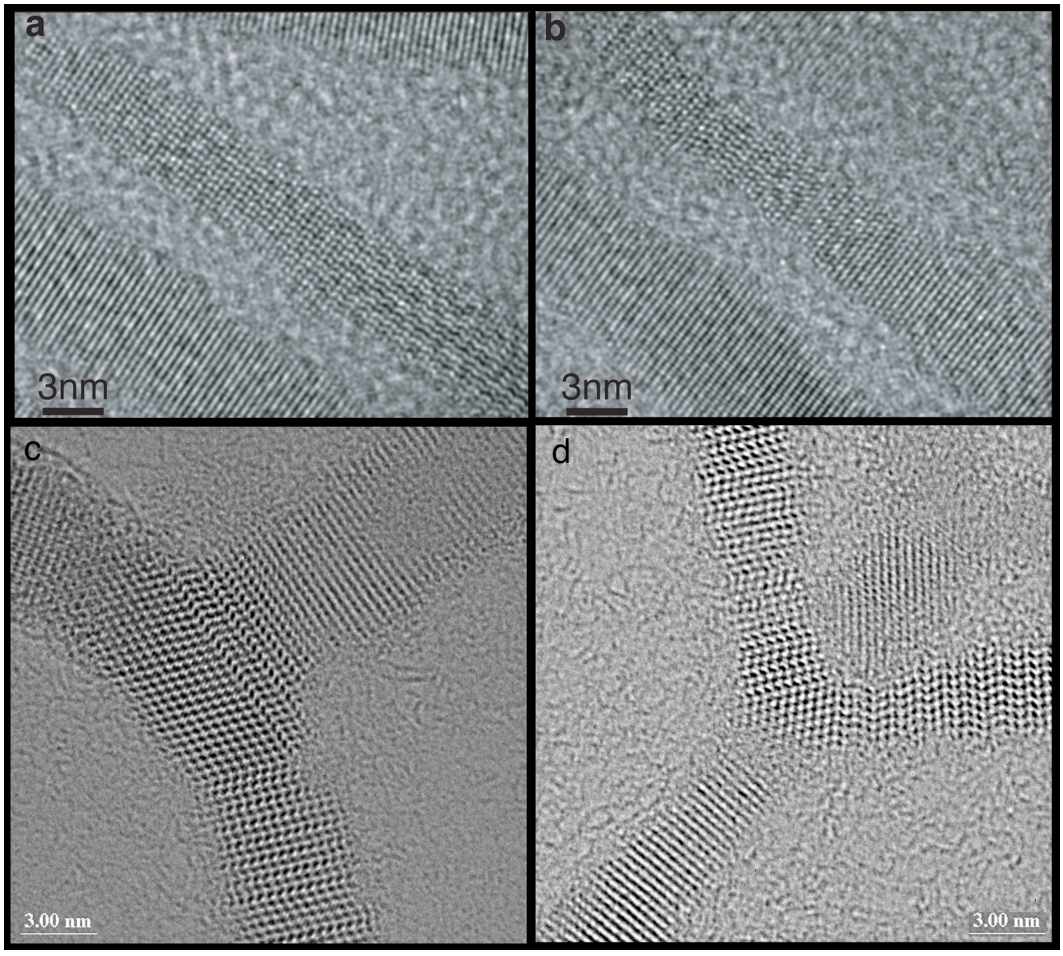

Figure 19. HRTEM images of various heterojunctions. CdS nanorods with CdTe extensions (a and b) clearly show that these structures can grow epitaxially despite a large 11% lattice mismatch. In CdSe/CdTe heterostructures, branch points form at a heterojunction when zinc blende is nucleated at the end of the initial rod followed by wurzite arm growth (c and d).

4.4.5. Branched Rod Growth Directions

We can use the method outlined in Chapter 3 for identifying growth directions by stacking fault density as a means to further characterize the branched heterostructures. By identifying which end is fast growing which is the slow growing face, we can determine if these factors play a role in the heterostructure's branching. In the structures whish were examined and shown in Figure 20, CdTe is grown off the ends of CdSe nanorods. In all of the branched structures that were examined it was found that the zinc blende segment is grown off of the fast growing, fault free, (00-1) face, while the linear segment is grown off the (001) face, responsible for the fault rich region of the CdSe nanorod. While unconfirmed, this behavior is likely due to the material being able to reach its thermodynamically favorable structure uninhibited on the fast growing face, which for CdTe is zinc blende[10]. Meanwhile on the slow growing face, the new material is trapped between crystal phases just like the CdSe, therefore highly faulted in the linear wurtzite phase.

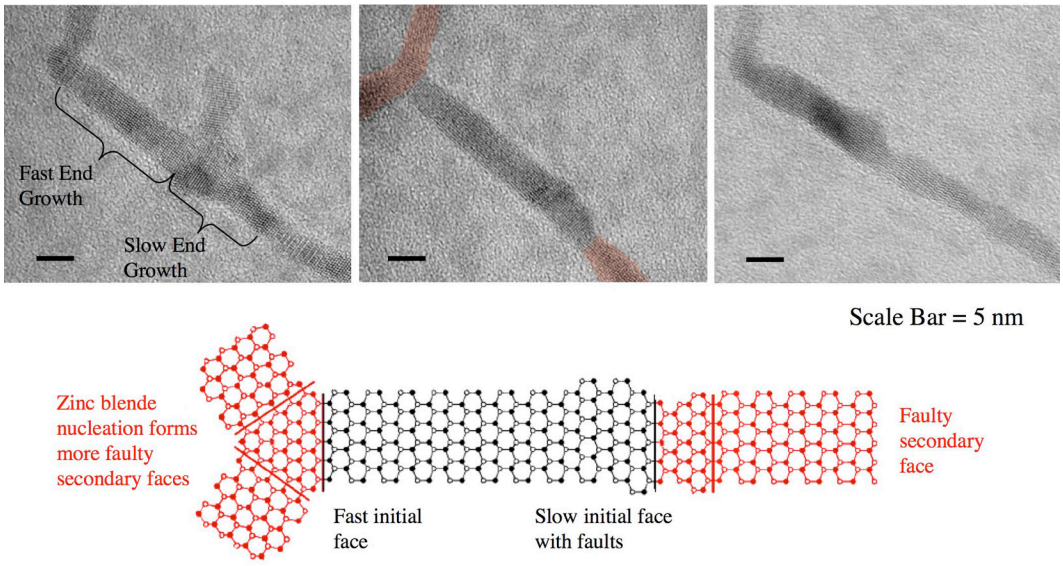

Figure 20. HRTEM images and model of CdSe/CdTe nanocrystal heterostructures. From the images, one can see the distinct regions as laid out in the model, an inner CdSe rod with regions of CdTe grown off the ends (highlighted in red in the center image). Observing the inner rod's two regions, one can see that the linear extension grows from the slow growing (001) face and tends to be highly faulted, while the branched end grows from the initial fast growing (00-1) face of the CdSe.

4.4.6. Theoretical Models

Our approach to synthesizing nanocrystal heterostructures can not only create solution processible analogues of nanowire heterostructures, but also enables unique functionality through the three dimensional arrangement of components. Representative heterostructures reported here incorporate either Type I or Type II interfaces to define the nature of the interactions between components. In the first case, CdSe extensions grown on a CdS nanorod are quantum rods separated by a barrier for electrons and holes, Figure 21. The coupling of these rods is tuneable by changing the length of the original rod or of the extensions, or selecting a different material to vary the barrier height. *Ab initio* calculation of the electronic structure of these heterostructures confirms that the lowest energy level is split into "symmetric" and "anti–symmetric" combinations. A coupling energy of 27 meV was estimated for a heterostructure with a three monolayer CdS barrier (three layers each of Cd and S) and this coupling energy drops to 9 meV when the CdS barrier is six monolayers thick. Such tuneable coupling, combined with the long spin coherence times observed in colloidal nanocrystals[62], make these heterostructures intriguing candidates for control of quantum coherence.

The theoretical calculations were done using the charge patching method[63]. This method calculates the band edge states of a nanosystem with *ab initio* accuracy, but scales linearly to the size of the system. The surface of a nanosystem is passivated with pseudo–hydrogen atoms, e.g., one pseudo–hydrogen atom with nuclear charge Z=1.5 electron for each Cd dangling bond, and Z=0.5 electron for each Se, S, or Te dangling bond. This simple model represents an ideal passivation which captures the essence of

any good experimental passivations. The atomic positions of a given passivated binary semiconductor nanosystem (i.e., CdSe/CdTe, CdSe/CdS) are relaxed using the valence force field (VFF) method. This atomistic method describes the elastic aspects of the system accurately. After the atomic positions of a given system are determined, small prototype systems are precalculated under the local density approximation (LDA) of the density functional theory. The charge densities of these small prototype systems are used to generate localized charge motifs around each atom. The charge motifs for bulk Cd, Se, Te, S atoms and surface pseudo–hydrogen atoms, and the derivatives of these charge motifs regarding the change of bond lengths and bond angles are all generated. Then, these charge motifs and their derivatives are placed together to generate the LDA charge density of a given nanosystem[63]. The typical error of the so generated charge density compared to the directly calculated charge density under LDA is about 1%. The resulting eigenstate error is about 20–40 meV. The energy splittings between states within the conduction or valence band have typical errors of a few meV. After the charge density is obtained, LDA formulae are used to calculate the LDA total potential and the LDA Hamiltonian. Then the folded spectrum method[64, 65] is used to calculate the band edge states. Under this procedure, the *ab initio* accuracy band edge states of a thousand atom nanosystem can be calculated within a few hours on a parallel computer. To calculate coupling energies, a small external electrical field was applied to cancel the permanent dipole of the nanorod[66]. The diameter of the calculated rod shown in Fig. 21a is about 2 nm, the total length is about 9.5 nm, and there are in total 2002 atoms. For the calculated tetrapod in Fig. 21b, each branch has a diameter of 2.2 nm and a length of 4.2 nm. There are in total 3685 atoms in the tetrapod.

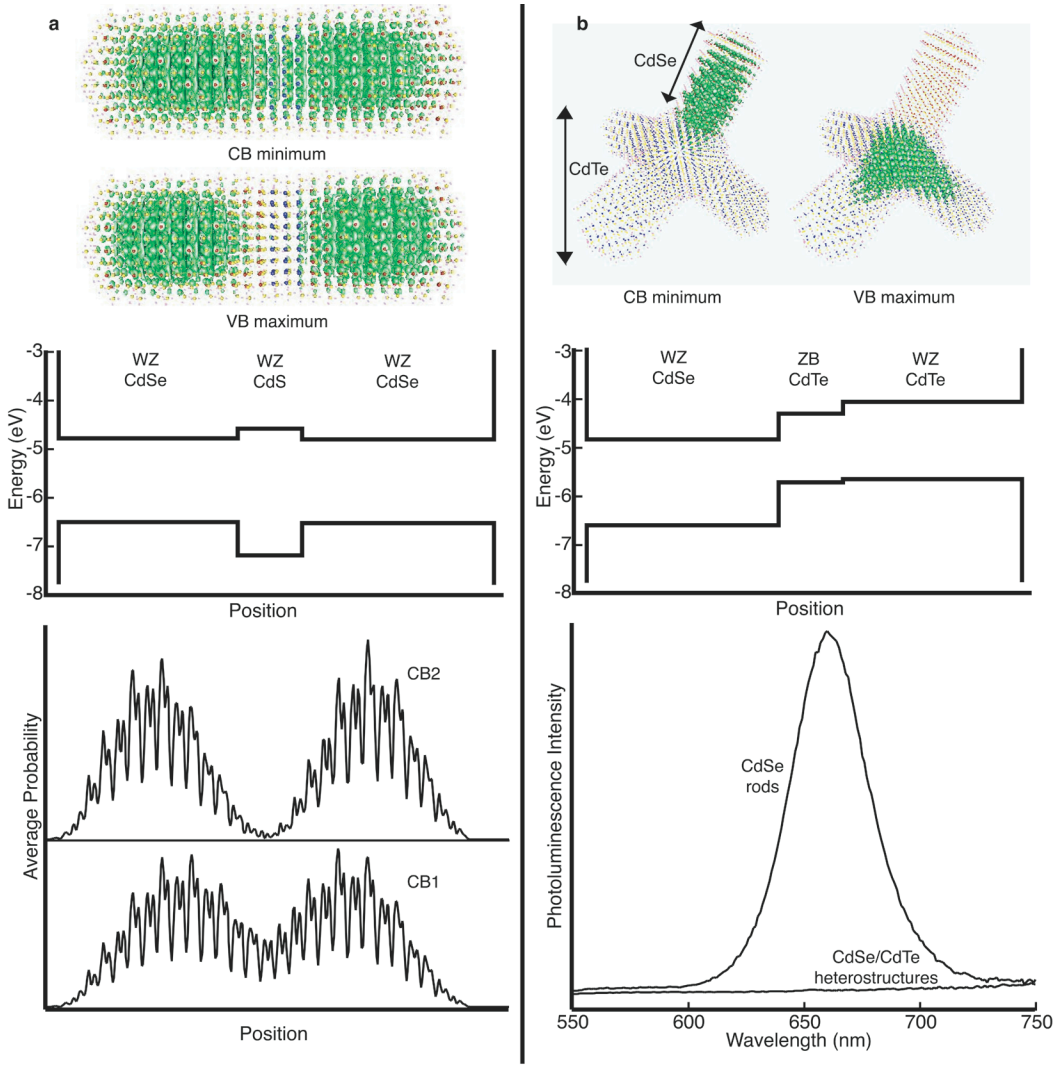

Figure 21. Optoelectronic properties of Type I and Type II heterostructures. **a**, *Ab initio* calculation of Type I CdSe/CdS/CdSe heterostructures reveals electronic coupling. Isosurfaces of the lowest energy electron and highest energy hole states (top) show the even distribution of probability between the two terminal CdSe quantum rods. The band alignment illustrates the formation of coupled wells for electrons and holes. The cross section–averaged probability for the lowest energy conduction band state (CB1) shows significant penetration of the CdS barrier, while the next conduction band state (CB2) has a longitudinal node. The diameter of the calculated rod is about 2 nm, the total length is

about 9.5 nm, and there are in total 2002 atoms. The thickness of the CdS is three monolayers. **b**, In Type II CdSe/CdTe heterostructures the electron and hole are spatially separated. Their distribution agrees qualitatively with the expected band alignment. The photoluminescence of the CdSe rods immediately before adding CdTe branches is easily observed (bottom), while in heterostructures, charge separation strongly quenches the luminescence. For the calculated tetrapod, each branch has a diameter of 2.2 nm and a length of 4.2 nm. There are in total 3685 atoms in the tetrapod.

4.5. Conclusion

Branched tetrapods with CdSe central tetrapods and terminal CdTe branches are interesting for their unusual charge separating properties. These structures absorb light across the visible spectrum, then separate electrons and holes across their Type II interfaces. The sharp reduction in spatial overlap between electrons and holes, apparent in the *ab initio* result, effectively quenches the band gap photoluminescence, Figure 21b. Both CdSe rods and CdTe tetrapods emit well–defined band gap luminescence under similar conditions. Calculations have furthermore suggested that electrons localize in the zinc blende core of CdSe tetrapods[67]. In the heterostructured branched tetrapods, Figure 12, this implies long range charge separation with the electron at the CdSe zinc blende core and the hole delocalised in the outer CdTe branches, 30 nm or more away. This distance can be tuned by the changing dimensions of the central tetrapod. Organic dendrimers designed for such radial charge separation[68] required three generations of growth and purification to separate charges by only a few nanometers. The nature and lifetime of this proposed charge separated state is currently under investigation, as are possible applications to photovoltaic energy conversion.

Additionally, we've also learned that the +/-(001) faces on the ends of the nanorods play a role in branching. The branched rod heterostructures have demonstrated that the chemistry of the crystal face plays as much a role in branching as the other synthesis conditions such as temperature or concentration. Proper branch points consisting of a zinc blende core only formed on the fast growing (00-1) face. Erratic branching and 'back branching' was found on the linear extension of both branched rods and extended

arm tetrapods, but these were due to high energy faces forming due to the large number of stacking faults at these locations, and were neither controllable or predictable.

Chapter 5. Oriented Attachment

5.1. Introduction

The heterostructures outlined in Chapter 4 are not the only means to create branched nanoparticles from a batch of nanorods. For years the process of oriented attachment with nanocrystals has been investigated for its potential to simplify the growth process[69-72]. In oriented attachment, the goal is to use existing particles as the building blocks for ultimately more complex structures by controllably joining the initially pieces in an ordered fashion. Inorganic semiconducting nanocrystals are ideal for an oriented attachment system because they are about as small a building block one can get in identifiable shapes such as spheres, rods, or even the tetrapods[3]. There is great interest in the use of these materials in the miniaturization of computing and electronics partly due to their shape and size control as outlined earlier in the introduction, but even greater control by oriented attachment would increase their viability. Demonstrated here is a system to systematically extend rods and form junctions at discrete angles by the process of oriented attachment assisted through deposition and subtraction of gold at the tips of CdSe nanorods[73-75].

5.2. Synthetic Methods

The method of attachment developed here is a three step process as outlined in figure 22. In the first step shown in 22A, the rods are gold tipped by the standard double tipping technique previously reported in Chapter 2. In the second step, 1B, the rods are

gently refluxed in toluene to encourage the aggregation of the gold tips. The ideal time was found to be approximately 2 hrs, less than this and the majority of rods remained unjoined, but too long and there will be excessive aggregation. The final step, 22C, is the removal of gold by refluxing the rods in an excess of toluene and thiophenol. It is possible to use this method of oriented attachment as an iterative process, but with limitations. The length of the attached structures and the amount of branching increases when the process is cycled more than once. However, as the structures become more complex the likelihood irreversible aggregation by the gold increases as well, Figure 23.

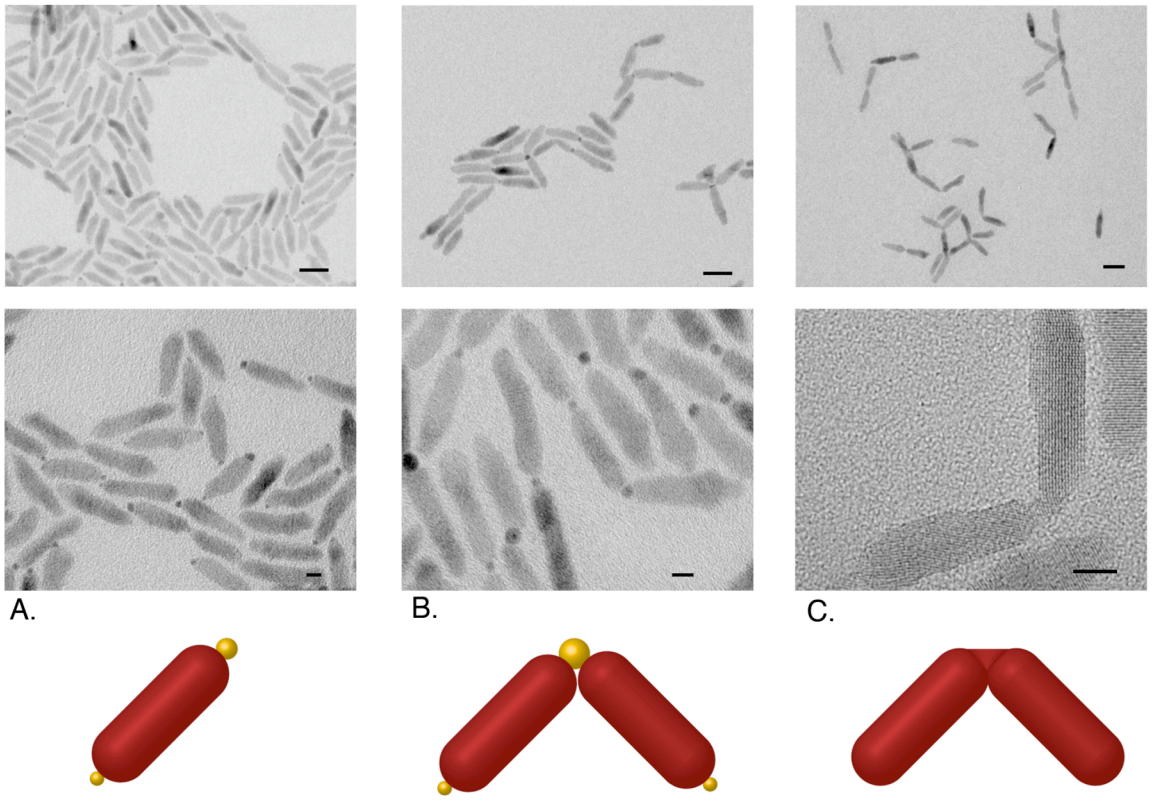

Figure 22. In the above experiment,(A) CdSe rods were initially tipped with gold. (B) These rods were then heated in toluene to encourage the aggragation of the gold tips. (C) Finally the rods were refluxed with thiophenol in the presence of Cd precurser to leave the rods joined while removing the gold. Scale bars all equal 20 nm.

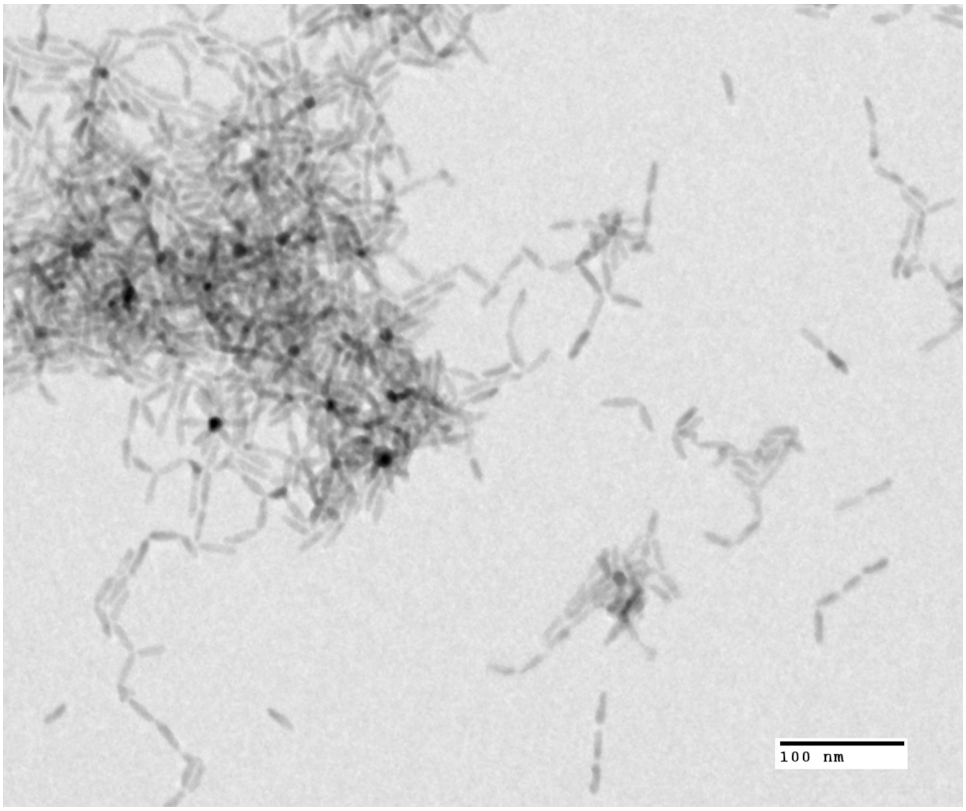

Figure 23. After multiple iterations of the attachment process, it is easy to create irreversible aggregation via the gold tips. This image is after only two iterations of attachment, the majority of the gold was removed from the rods, however, there were islands of aggregation such as the one in the upper left of this image.

5.3. Attachment Characterization

5.3.1. Presence of Gold

High resolution transmission electron microscopy was the primary means of characterization for the attachment process. As shown in Figure 24a, after tipping, the lattice spacing of the bead at the end of the rod matches that of the (111) planes of gold. After refluxing, figure 24b shows that the aggregation of the gold tips is a non specific process, forming a large grain boundary between the two gold tips. Finally, in Figure 24c it is clear that after refluxing in thiols, there is no gold present between the two rods. At this point the attachment is now an epitaxially grown segment of CdSe between the two rods, in this case in the zinc blende phase.

5.3.2. Orientation of Gold Tipping

Using the technique outlined in Chapter 3 for determining crystal orientation by stacking fault distribution, it has been found that there is preferential growth of gold on one end of the nanorod initially, Figure 25. In a short survey of approximately 25 rods, all single tipped rods had gold on the fast growing face. As growth continued the gold eventually appeared on both ends, but the larger of the two gold tips was still at the end of the fast growing, fault free region, indicating it had been growing for a longer duration.

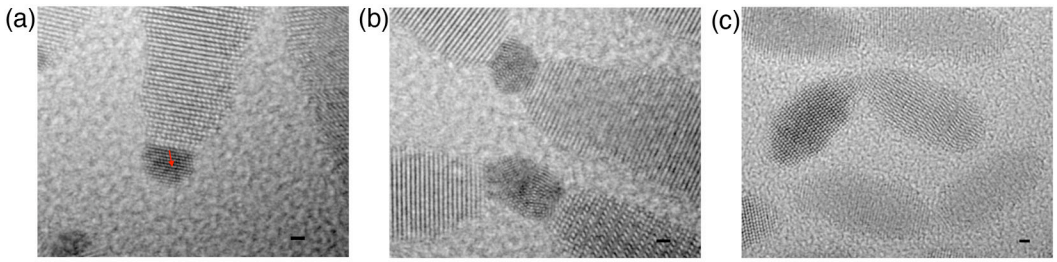

Figure 24. (a) A gold sphere at the tip of a rod with lattice spacings matching that of the (111) face of gold, 2.38 Å, in the indicated direction. (b) Two sets of gold spheres joining two CdSe rods. (c) Two rods joined by a section of zinc blende CdSe after the subtraction of gold. Scale bars are 1 nm.

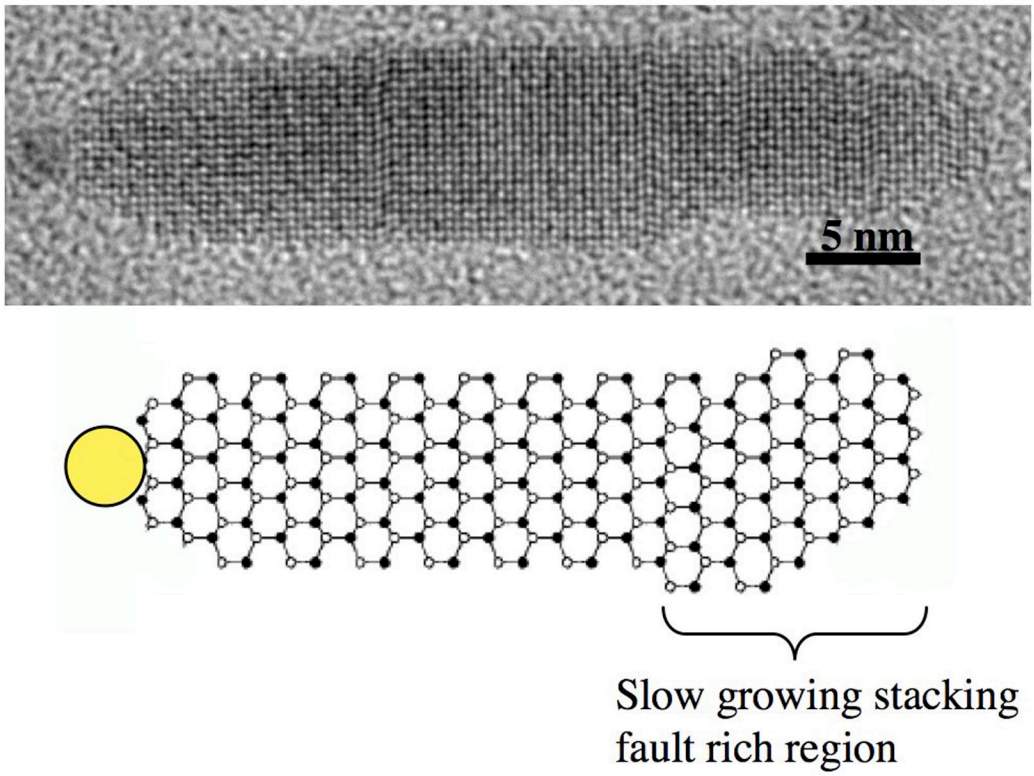

Figure 25. HRTEM imge and schematic of a single gold tipped CdSe nanorod. As the schematic highlights, the gold tip forms on the fast growing, less faulty, end of the rod.

5.3.3. Attachment Directionality

After the final attachment step, there are three orientations that may occur, shown in Figure 26, which can be elucidated using the method outlined in Chapter 3. The first scenario, 26a, is that two rods are joined with two (00-1) faces coming together. In this scenario, the interface between the rods is disordered due to the necessary reconstruction of atoms. In the second scenario, 26b, the (00-1) face of one rod meets the (001) face of the second rod. Here the two faces properly match each other and either a small linear section of wurtzite or zinc blende can bridge the two rods. In the final scenario, 26c, two or three rods are at an angle from each other with (00-1) faces meeting before the gold is removed. Once the gold is removed, a zinc blende section of CdSe is formed allowing for two or three rods to be easily joined.

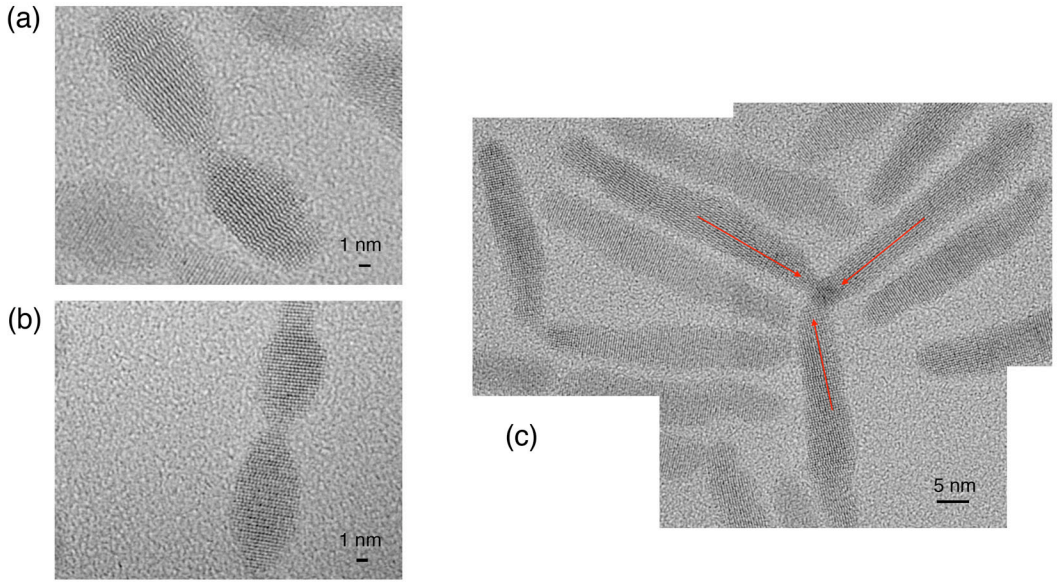

Figure 26. When two rods join together with like faces in a linear fashion the interface is difficult to image do to structural rearrangements (a). However, when two rods join with opposite faces in a linear fashion the interface is most often a wurtzite structure (b). When two or three rods join at an angle, the interface is clearly CdSe zinc blende (c). In this case the image is a composite of three separate TEM images, and shows three rods joined by the equivalent (111) faces of the zinc blende at the center.

5.3.4. Distribution of Angles Before and After Attachment

The attachment process between the last two steps increases the order of the system. During the last step, the rods go from being nonspecifically aggregated by gold to epitaxially attached at discrete angles via crystalline growth. This can be observed in the distribution of angles between rods shown in Figure 27. Before gold removal there is a largely random distribution of rod-rod angles between 90 and 180 degrees. Once the gold is removed, the angle between rods that remain attached is now governed by the presence of either wurtzite or zinc blende at the joint. If the new segment is wurtzite, the angle is 180 degrees, but if there is zinc blende the angle will be approximately 109.5 degrees. The zinc blende angle will vary depending on how the crystal is lying on the substrate since the angle measured is that of a 2-dimensional projection.

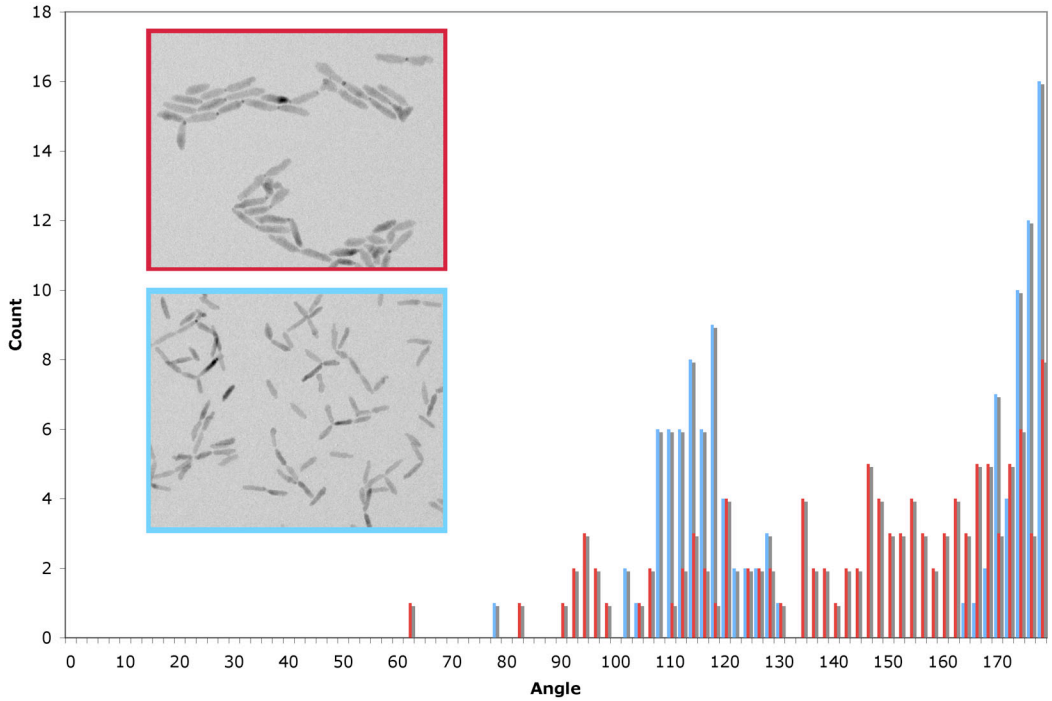

Figure 27. The distribution of angles between two joined rods before and after the removal of gold from the joint. When gold is at the joint between two rods (red) there is a random distribution of angles between the two rods due to the nonspecific aggregation of the gold spheres. After the removal of the gold (blue), the angles are dictated by either the presence of wurtzite, 180^{o}, or zinc blende, 109.5^{o}.

5.3.5. Possible Heterostructure Formation

Originally, this method was being investigated as an alternative means of heterostructure formation as well as means of branching. For this purpose, the attachment method was also tried on both CdS and CdTe nanocrystal, unfortunately each posed their own difficulties. Unlike CdSe, the tipping process with CdS was far more aggressive, tipping not only the ends, but rather covering the rods with small gold dots, Figure 28a. This led to difficulties joining the rods by the attachment process, because the rods would only join when brought end to end. With gold covering the rods they would aggregate in too many alternative orientations. Once the gold was removed the rods would simply fall apart from each other. Meanwhile, CdTe was simply too reactive with the gold, appearing to alloy immediately after the initial gold addition, Figure 28b. After this occurred, the gold did not aggregate as before, and could not be removed by refluxing in thiols.

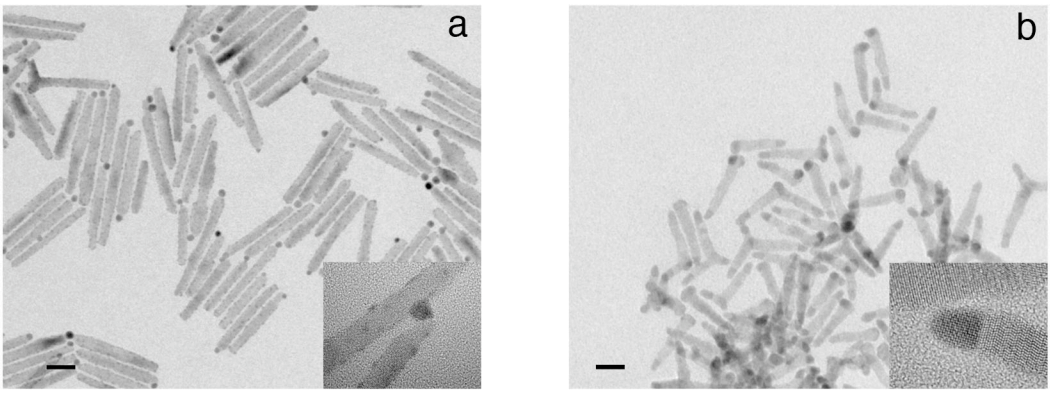

Figure 28. Other common chalcoginides posed unique problems for oriented attachment. Gold tipping on CdS was less selective than CdSe, tipping on the sides as well as the ends, leading to misdirected gold aggregation (a). In CdTe, the gold did not form beads on the rods ends, but appeared to diffuse into the CdTe possibly forming an alloy (b). Scale bars equal 20 nm.

5.4. Conclusion

Using this method of oriented attachment, one can easily combine simple CdSe nanorods together to form systems of greater complexity. The gold that is added into the system is used only in an intermediate step, so that the resulting structures are completely CdSe. Additionally, the final joining material is CdSe grown epitaxially, so the resulting structure is completely crystalline. Because of these features, this method could prove useful in the integration of semiconductor nanocrystals in future electronics.

Chapter 6. Concluding Remarks

This work has demonstrated new methods for creating and characterizing advanced branching semiconducting nanocrystals. By further developing control over these structures they will become more viable materials in a world of miniaturizing technology. All the structures discussed in this body of work are solution processable and easily scaled making them ideal for integration into larger systems.

The first step in this process was further understanding how the basic anisotropic rod grows, and how stacking faults form in a rod due to these materials' polytypism. It was found that the fault growth is anisotropic, forming preferentially on the (001) face during rod growth. This face is responsible for the growth of approximately 40% of a typical CdSe rod grown using CdO as a precursor. Other materials and growth methods have different ratios of growth between the two end faces, however the majority of the fault growth appears to be due to the slower growing face. Thus we have the picture of a nanorod comprised of two primary sections: the larger fault free side due to the fast growing (00-1) face makes up between 60-80% of the nanorod, and the smaller fault rich side due to the (001) face making up between 20-40% of the nanorod.

Additionally, using the technique of identifying the fast (00-1) and slow (001) growing faces by stacking faults allows for easy qualitative analysis of rods in more complex systems. Using this technique, it is possible to determine that during the growth of branched rod heterostructures, the nucleation of zinc blende on the branching end takes

place on the fast growing (00-1) face. During the growth of gold tips on the ends of CdSe nanorods, it is also possible to determine that tipping also begins on the (00-1) face.

Meanwhile, two techniques for creating complex branched structures were also outlined in this dissertation. The first is a method of forming complex linear and branched heterostructure nanocrystals. These crystals consist of an original rod or tetrapod nanocrystal upon which a second material is grown from the ends, either linearly or branched. The structures can be grown in a single pot synthesis due to the two materials sharing a common cation, cadmium. The introduction of the anion by injection begins the nucleation and growth of the nanocrystals, and after consuming the original anion, the second material's growth begins with the injection of another anion precursor. Because of the polytypism, four main structures can be formed as outlined in Figure 11.

These materials are interesting not only because of their shape, but also due to their charge separation ability. After absorbing light, the electron and hole pair are separated due to the type II interface between the two materials. Experiment and *ab initio* calculations have demonstrated a complete quenching of any band gap photoluminescence due to this separation. Coupled with their unique shapes, these materials should be very interesting for industrial integration and application in such fields as photovoltaic energy conversion.

Finally, it has been shown that along with epitaxial growth, oriented attachment is a viable option for the formation of branched nanocrystals. In this technique, gold tipping the rods was used as an intermediate means to join the rods. At this stage the rods, while joined by the gold, show no preferential orientation besides the end to end attachment. Only after the removal of the gold and the epitaxial growth of a bridge

between the two rods are they now a new single nanocrystal. Depending on the orientation and number of original rods joined by the gold, the new bridging material may be either wurtzite or zinc blende after the gold's subtraction.

The work presented here has already contributed to the way nanocrystals are perceived and used. New techniques and applications are being thought up daily to further our knowledge and understanding of these nanomaterials, and every bit helps. Understanding how the materials grow, and the ability to easily characterize them once integrated into larger systems will be key in the future of these nanostructures. Knowing that one end of the rod is responsible for the growth of stacking faults can lead to future work in shutting down the growth on that face to create perfect crystals. The success of the heterostructures shown here will hopefully create new materials that integrate multiple materials at the earliest stages of growth for easier integration and processability. The work with oriented attachment work has also demonstrated that there is no one method for the formation of branched materials, and that each technique will bring with it new possibilities. When a means to integrate multiple materials with this process is found it will yield new heterostructures that cannot otherwise be formed. Every step down the road leads to new opportunities, and with any luck those will bring even more.

References

1. Peng, X.; Manna, L.; Yang, W.; Wickham, J.; Scher, E. C.; al., e., Shape control of CdSe nanocrystals. In *Nature*, 2000.

2. Peng, Z. A.; Peng, X., Nearly Monodisperse and Shape-Controlled CdSe Nanocrystals via Alternative Routes: Nucleation and …. In *Science*, 2001.

3. Manna, L.; Scher, E. C.; Alivisatos, A. P., Synthesis of Soluble and Processable Rod-, Arrow-, Teardrop-, and Tetrapod-Shaped CdSe Nanocrystals. In *Langmuir*, 1999.

4. Scher, E. C., Shape control and applications of nanocrystals. In *Philosophical Transactions: Mathematical*, 2003.

5. Moore, D.; Ronning, C.; Ma, C.; Wang, Z., Wurtzite ZnS nanosaws produced by polar surfaces. In *Chemical Physics Letters*, 2004.

6. Murray, C. B.; Norris, D. J.; Bawendi, M. G., Synthesis and characterization of nearly monodisperse CdE (E= sulfur, selenium, tellurium) …. In *Journal of the American Chemical Society*, 1993.

7. Colvin, V. L.; Alivisatos, A. P.; Tobin, J. G., Valence-band photoemission from a quantum-dot system. In *Physical Review Letters*, 1991.

8. Yin, Y.; Alivisatos, A. P., Colloidal nanocrystal synthesis and the organic-inorganic interface. In *Nature*, 2005.

9. Li, L. s.; Hu, J.; Yang, W.; Alivisatos, A. P., Band Gap Variation of Size- and Shape-Controlled Colloidal CdSe Quantum Rods. *Nano Lett.* **2001,** 1, (7), 349-351.

10. Yeh, C. Y.; Lu, Z. W.; Froyen, S.; Zunger, A., Zinc-blende–wurtzite polytypism in semiconductors. In *Physical Review B*, 1992.

11. Takeuchi, S.; Suzuki, K., Stacking Fault Energies of Tetrahedrally Coordinated Crystals. In *Physica Status Solidi (A*, 1999.

12. Manna, L.; Milliron, D. J.; Meisel, A.; Scher, E. C.; al., e., Controlled growth of tetrapod-branched inorganic nanocrystals. In *Nature Materials*, 2003.

13. Wei, S. H.; Zunger, A., Calculated natural band offsets of all II–VI and III–V semiconductors: Chemical trends and the role …. In *Applied Physics Letters*, 1998.

14. Alivisatos, A. P., Perspectives on the Physical Chemistry of Semiconductor Nanocrystals. In *J. Phys. Chem*, 1996.

15. Moore, G. E., Lithography and the future of Moore's law. In *Proceedings of SPIE*, 2003.

16. Sone, J.; Fujita, J.; Ochiai, Y.; Manako, S.; Matsui, S.; al., e., Nanofabrication toward sub-10 nm and its application to novel nanodevices. In *Nanotechnology*, 1999.

17. Chan, E. M.; Mathies, R. A.; Alivisatos, A. P., Size-Controlled Growth of CdSe Nanocrystals in Microfluidic Reactors. *Nano Lett.* **2003,** 3, (2), 199-201.

18. Cao, Y. W.; Banin, U., Growth and Properties of Semiconductor Core/Shell Nanocrystals with InAs Cores. In *Science*, 1998.

19. Trindade, T.; PO'Brien; Pickett, N. L., Nanocrystalline semiconductors: synthesis, properties, and perspectives. In *Chem. Mater*, 2001.

20. Li, Z.; Xie, Y.; Xiong, Y.; Zhang, R.; He, W., Reverse Micelle-assisted Route to Control Diameters of ZnO Nanorods by Selecting Different …. In *Chemistry Letters*, 2003.

21. Wu, Q.; Zheng, N.; Ding, Y.; Li, Y., Micelle-template inducing synthesis of winding ZnS nanowires. In *Inorganic Chemistry Communications*, 2002.

22. YU, W. W.; Wang, Y.; Peng, X., Formation and stability of size-, shape-, and structure-controlled CdTe nanocrystals: Ligand effects …. In *CHEMISTRY OF MATERIALS*, 2003.

23. Tolbert, S. H.; Alivisatos, A. P., Size Dependence of a First Order Solid-Solid Phase Transition: The Wurtzite to Rock Salt …. In *Science*, 1994.

24. Yin, Y.; Rioux, R. M.; Erdonmez, C. K.; Hughes, S. M.; al., e., Formation of Hollow Nanocrystals Through the Nanoscale Kirkendall Effect. In *Science*, 2004.

25. Son, D. H.; Hughes, S. M.; Yin, Y.; Paul Alivisatos, A., Cation Exchange Reactions in Ionic Nanocrystals. In *Science*, 2004.

26. Mews, A.; Eychmueller, A.; Giersig, M.; Schooss, D.; al., e., Preparation, characterization, and photophysics of the quantum dot quantum well system cadmium …. In *The Journal of Physical Chemistry*, 1994.

27. Mekis, I.; Talapin, D. V.; Kornowski, A.; Haase, M.; al., e., One-pot synthesis of highly luminescent CdSe/CdS core–shell nanocrystals via organometallic and" …. In *J. Phys. Chem. B*, 2003.

28. Klein, D. L.; Roth, R.; Lim, A. K. L.; Alivisatos, A. P.; al., e., A single-electron transistor made from a cadmium selenide nanocrystal. In *Arxiv preprint cond-mat*, 1997.

29. Bruchez, M.; Moronne, M.; Gin, P.; Weiss, S.; Alivisatos, A. P., Semiconductor nanocrystals as fluorescent biological labels. In *Science*, 1998; Vol. 281, pp 2013-6.

30. Liddle, J. A.; Cui, Y.; Alivisatos, P., Lithographically directed self-assembly of nanostructures. In *J. Vac. Sci. Technol. B*, 2004.

31. Cui, Y.; Banin, U.; Björk, M. T.; Alivisatos, A. P., Electrical Transport Through a Single Nanoscale SemiconductorBranch Point. In *Nano Letters*, 2005.

32. Gorostiza, P.; Aruguete, D. M.; Bastus, N. G.; Alivisatos, A. P., Collective behaviour in two-dimensional cobalt nanoparticle assemblies observed by magnetic force …. In *Nat Mater*, 2004.

33. Wei, S. H.; Zhang, S. B.; Zunger, A., First-principles calculation of band offsets, optical bowings, and defects in CdS, CdSe, CdTe, and …. In *Journal of Applied Physics*, 2000.

34. Thelander, C.; Mårtensson, T.; Björk, M. T.; Ohlsson, B. J.; al., e., Single-electron transistors in heterostructure nanowires. In *Applied Physics Letters*, 2003.

35. Li, L. S.; Alivisatos, A. P., Semiconductor Nanorod Liquid Crystals and Their Assembly on a Substrate. In *Advanced Materials*, 2003.

36. Williams, D. B. a. C., C.B., *Transmission Electron Microscopy*. 1996.

37. Wang, Z., Transmission electron microscopy of shape-controlled nanocrystals and their assemblies. In *J. Phys. Chem. B*, 2000.

38. Suzuki, K.; Ichihara, M.; Takeuchi, S., High-resolution electron microscopy of extended defects in wurtzite crystals. In *Japanese Journal of Applied Physics*, 1994.

39. Suzuki, K.; Takeuchi, S.; SHINO, M.; KANAYA, K.; IWANAGA, H., Lattice image observations of defects in CdS and CsSe. In *Transactions of the Japan institute of metals*, 1983.

40. Ricolleau, C.; Audinet, L.; Gandais, M.; Gacoin, T., Structural transformations in II-VI semiconductor nanocrystals. In *The European Physical Journal D-Atomic*, 1999.

41. Tonti, D.; van Mourik, F.; Chergui, M., On the Excitation Wavelength Dependence of the Luminescence Yield of Colloidal CdSe Quantum Dots. In *Nano Lett*, 2004.

42. Hiisselbartb, A.; Giersig, M.; Weller, H., Chemistry and Photophysics of Mixed CdS/HgS Colloids. In *J. Phys. Chem*, 1993.

43. Madhukar, A.; Lu, S.; Konkar, A.; Zhang, Y.; Ho, M.; al., e., Integrated semiconductor nanocrystal and epitaxical nanostructure systems: structural and optical …. In *Nano Lett*, 2005.

44. Milliron, D. J.; Hughes, S. M.; Cui, Y.; Manna, L.; Li, J.; Wang, L.-W.; Paul Alivisatos, A., Colloidal nanocrystal heterostructures with linear and branched topology. *Nature* **2004,** 430, (6996), 190-195.

45. Li, J.; Wang, L. W., Electronic Structure of InP Quantum Rods: Differences between Wurtzite, Zinc Blende, and Different …. In *Nano Lett*, 2004.

46. Manna, L.; Scher, E.; Li, L. S.; Alivisatos, A. P., Epitaxial growth and photochemical annealing of graded CdS/ZnS shells on colloidal CdSe nanorods. In *J. Am. Chem. Soc*, 2002.

47. Manna, L.; Wang, L. W.; Cingolani, R.; Alivisatos, A. P., First-principles modeling of unpassivated andsurfactant-passivated bulk facets of wurtzite CdSe: A …. In *Journal of Physical Chemistry B*, 2005.

48. Huynh, W. U.; Dittmer, J. J.; Alivisatos, A. P., Hybrid Nanorod-Polymer Solar Cells. In *Science*, 2002.

49. Kazes, M.; LEWIS, D. K.; Ebenstein, Y.; Mokari, T.; Banin, U., Lasing from Semiconductor Quantum Rods in a Cylindrical Microcavity*. In *Phys. Lett*, 2001.

50. Schedelbeck, G.; Wegscheider, W.; Bichler, M.; al., e., Coupled Quantum Dots Fabricated by Cleaved Edge Overgrowth: From Artificial Atoms to Molecules. In *Science*, 1997.

51. Bayer, M.; Hawrylak, P.; Hinzer, K.; Fafard, S.; al., e., Coupling and Entangling of Quantum States in Quantum Dot Molecules. In *Science*, 2001.

52. Gudiksen, M. S.; Lauhon, L. J.; Wang, J.; Smith, D. C.; al., e., Growth of nanowire superlattice structures for nanoscale photonics and electronics. In *Nature*, 2002.

53. Collier, C. P.; Vossmeyer, T.; Heath, J. R., NANOCRYSTAL SUPERLATTICES. In *Annual Review of Physical Chemistry*, 1998.

54. Ouyang, M.; Awschalom, D. D., Coherent Spin Transfer Between Molecularly Bridged Quantum Dots. In *Science*, 2003.

55. Hines, M. A.; Guyot-Sionnest, P., Synthesis and characterization of strongly luminescing ZnS-capped CdSe nanocrystals. In *J. Phys. Chem*, 1996.

56. DABBOUSI, B. O.; RODRIGUEZ-VIEJO, J.; MIKULEC, F. V.; al., e., (CDSE) ZNS CORE-SHELL QUANTUM DOTS: SYNTHESIS AND CHARACTERIZATION OF A SIZE SERIES OF HIGHLY …. In *The Journal of physical chemistry. B*, 1997.

57. Peng, X.; Schlamp, M. C.; Kadavanich, A. V.; Alivisatos, A. P., Epitaxial growth of highly luminescent CdSe/CdS core/shell nanocrystals with photostability and …. In *J. Am. Chem. Soc*, 1997.

58. Kim, S. C.; Fisher, B.; Eisler, H. J.; Bawendi, M. G., Type-II quantum dots: CdTe/CdSe (core/shell) and CdSe/ZnTe (core/shell) heterostructures. In *J. Am. Chem. Soc*, 2003.

59. EYCHMÜLLER, A.; Mews, A.; Weller, H., A quantum dot quantum well: CdS/HgS/CdS. In *Chemical Physics Letters*, 1993.

60. Borchert, H.; Dorfs, D.; McGinley, C.; Adam, S.; MÖLLER, T.; al., e., Photoemission study of onion like quantum dot quantum well and double quantum well nanocrystals of …. In *J. Phys. Chem. B*, 2003.

61. Mokari, T.; Banin, U., Synthesis and Properties of CdSe/ZnS Core/Shell Nanorods. In *J. Chem. Phys*, 2002.

62. Gupta, J. A.; Awschalom, D. D.; Peng, X.; Alivisatos, A. P., Spin coherence in semiconductor quantum dots. In *Physical Review B*, 1999.

63. Wang, L. W., Charge-Density Patching Method for Unconventional Semiconductor Binary Systems. In *Physical Review Letters*, 2002.

64. Wang, L. W.; Zunger, A., Solving Schrödinger's equation around a desired energy: Application to silicon quantum dots. In *The Journal of Chemical Physics*, 1994.

65. Canning, A.; Wang, L. W.; Williamson, A. J.; Zunger, A., Parallel Empirical Pseudopotential Electronic Structure Calculations for Million Atom Systems. In *Journal of Computational Physics*, 2000.

66. Li, L. S.; Alivisatos, A. P., Origin and Scaling of the Permanent Dipole Moment in CdSe Nanorods. In *Physical Review Letters*, 2003.

67. Li, J.; Wang, L. W., Shape effects on electronic states of nanocrystals. In *Nano Lett*, 2003.

68. Capistosti, G. J.; Cramer, S. J.; Rajesh, C. S.; Modarelli, D. A., Photoinduced electron transfer within porphyrin-containing poly (amide) dendrimers. In *Org. Lett*, 2001.

69. Zhao, L.; Lu, T.; Yosef, M.; Steinhart, M.; Zacharias, M.; Gosele, U.; Schlecht, S., Single-Crystalline CdSe Nanostructures: from Primary Grains to Oriented Nanowires. *Chem. Mater.* **2006,** 18, (26), 6094-6096.

70. Barnard, A. S.; Xu, H.; Li, X.; Pradhan, N.; Peng, X., Modelling the formation of high aspect CdSe quantum wires: axial-growth versus oriented-attachment …. In *Nanotechnology*, 2006.

71. Pradhan, N.; Xu, H.; Peng, X., Colloidal CdSe Quantum Wires by Oriented Attachment. In *Nano Lett*, 2006.

72. Yu, J. H.; Joo, J.; Park, H. M.; Baik, S. I.; Kim, Y. W.; Kim, S. C.; al., e., Synthesis of quantum-sized cubic ZnS nanorods by the oriented attachment mechanism. In *J. Am. Chem. Soc*, 2005.

73. Carbone, L.; Kudera, S.; Giannini, C.; Ciccarella, G.; al., e., Selective reactions on the tips of colloidal semiconductor nanorods. In *J. Mater. Chem*, 2006.

74. Mokari, T.; Sztrum, C. G.; Salant, A.; RABANI, E.; Banin, U., Formation of asymmetric one-sided metal-tipped semiconductor nanocrystal dots and rods. In *Nat Mater*, 2005.

75. Mokari, T.; Costi, R.; Sztrum, C. G.; RABANI, E.; Banin, U., Formation of symmetric and asymmetric metal-semiconductor hybrid nanoparticles. In *Physica status solidi. B. Basic research*, 2006.